Lawrence Berkeley National Laboratory
Recent Work

Title

STUDY OF w AND o PRODUCTION IN K+ p INTERACTIONS AT 4.6 AND 9.0 GeV/c

Permalink

https://escholarship.org/uc/item/5s77k02w

Authors

Alexander, G.
Firestone, A.
Fu, C.
et al.

Publication Date

1968-07-01

Cy. 2

University of California

Ernest O. Lawrence Radiation Laboratory

STUDY OF ω AND ϕ PRODUCTION IN K$^+$p INTERACTIONS
AT 4.6 AND 9.0 GeV/c

G. Alexander, A. Firestone, C. Fu, G. Goldhaber, and A. Pignotti

July 1968

Berkeley, California

E, P

DISCLAIMER

UNIVERSITY OF CALIFORNIA

Lawrence Radiation Laboratory
Berkeley, California

STUDY OF ω AND φ PRODUCTION IN K^+p INTERACTIONS AT 4.6 AND 9.0 GeV/c

G. Alexander, A. Firestone, C. Fu, G. Goldhaber, and A. Pignotti

July 1968

STUDY OF ω AND φ PRODUCTION IN K^+p INTERACTIONS
AT 4.6 AND 9.0 GeV/c[*]

G. Alexander, A. Firestone, C. Fu, G. Goldhaber, and A. Pignotti

Department of Physics and Lawrence Radiation Laboratory
University of California, Berkeley, California

ABSTRACT

We present results on the ω and φ production in $K^+p \rightarrow K^+\omega p$ and $K^+p \rightarrow K^+\varphi p$ interactions at incident momenta of 4.6 and 9.0 GeV/c. There is no statistically significant evidence for Kω or Kφ resonance production. The 437 $K^+\omega p$ events at 9 GeV/c are analyzed in terms of a multiperipheral Regge model on the entire Dalitz plot. The events have been assigned to the various peripheral diagrams on the basis of criteria in the four-momentum transfers. A satisfactory description of the data has been obtained on the basis of diagrams involving Pomeranchuk and meson exchanges.

I. INTRODUCTION

In the past, the Regge pole model, which has been relatively successful

in describing high energy two- and quasi-two-body reactions, has been extended

to multiparticle reactions.[1] In particular, there have been some recent

applications of the multiperipheral Regge pole model to three-body final state

reactions.[2-4] Because the Regge model was originally introduced as an asymptotic

expansion, in these works the model was used to fit only the comparatively

small fraction of events for which all two-particle subenergies were larger

than some prescribed values. In the case of the reactions $\pi p \to \rho \pi p$, Berger[5]

succeeded in extending the model down to threshold in the πp subenergy, but

was forced to perform a cut in the πN mass to avoid the strong presence of

the Δ resonance. Here we deal with the process $K^+ p \to K^+ \omega p$ in which no

strong resonances are observed, and we attempt a fit over the entire Dalitz

plot with a double Regge model. A justification of this attempt may be found

in the proposed extension of the Dolen-Horn-Schmid duality argument,[6] according

to which the multi-Regge formalism not only describes the asymptotic behavior

of the production amplitude, but also its behavior at lower energies, in some

average sense. If strong resonances are present, we cannot expect this average

description to be a precise one; on the other hand, if no resonant effects

are observed, it is tempting to try a detailed fit over the entire Dalitz

plot.

In the present work we have studied the production of ω and φ mesons in

$K^+ p$ interactions at 4.6 and 9.0 GeV/c in the final state configurations $K^+ \omega p$

and $K^+ \varphi p$. We attempt to describe in detail only the more abundant $K^+ \omega p$ channel

at 9 GeV/c in terms of the multiperipheral Regge pole model.

In Sec. II we describe the experimental procedure and results. In Sec. III we summarize the multiperipheral formalism used in this work and in Sec. IV discuss its application to the $K^+p \to K^+\omega p$ data at 9 GeV/c.

II. EXPERIMENTAL

The experiment was carried out with pictures taken in the 80-inch hydrogen bubble chamber at the Brookhaven National Laboratory alternating gradient synchrotron, exposed to an rf-separated K^+ beam. Some 50 000 pictures were taken with an incident K^+ beam momentum of 4.6 GeV/c and some 90 000 pictures with an incident momentum of 9 GeV/c. The four-prong events were measured with the LRL FSD and the remeasurements were carried out with a conventional digitizing machine. The events were then spatially reconstructed and kinematically fitted to the following possible final states:

$$K^+p \to K^+p\pi^+\pi^- \tag{1}$$
$$\to K^+p\pi^+\pi^-\pi^o \tag{2}$$
$$\to K^+n\pi^+\pi^+\pi^- \tag{3}$$
$$\to K^op\pi^+\pi^+\pi^- \tag{4}$$
$$\to K^+pK^+K^- \ . \tag{5}$$

For the 4.6-GeV/c events no difficulty was encountered in separating the various hypotheses by kinematical fit and ionization estimates. But at 9 GeV/c some events remained ambiguous even after these steps were taken. These ambiguous events were treated in the following way: (a) Events yielding a good fit to a four-constraint hypothesis [reactions (1) or (5)] and also to a one-constraint hypothesis [reactions (2), (3) or (4)] were considered to belong to the four-constraint hypothesis. (b) The remaining ambiguous events

were assigned to the hypothesis with the lowest chi-squared. The second

criterion might introduce some contamination in the final state of interest,

$K^+ p \pi^+ \pi^- \pi^0$, but this contamination is estimated to be small in the ω mass region

since the ω is a narrow resonance which is strongly produced. The three-pion

invariant mass distributions for the $K^+ p \pi^+ \pi^- \pi^0$ final state at 4.6 and 9 GeV/c

are shown in Fig. 1. Strong ω production is observed at both incident momenta

in the mass region 760 to 820 MeV. The $\omega \to \pi^+ \pi^- \pi^0$ decay distribution has

been investigated on the Dalitz plot and found to be in agreement with the

distribution of a 1^- meson decay plus the expected background. For comparison

the same analysis has been repeated for adjacent $\pi^+ \pi^- \pi^0$ mass regions where the

$\pi^+ \pi^- \pi^0$ decay distribution was found to be significantly different than in the

ω region. These results are shown in Fig. 2 in terms of the parameter λ

defined as

$$\lambda = \left| \frac{P_+ \times P_-}{Q^2} \right|^2$$

where $P_\pm$ are the momenta of the two charged decay pions in the ω rest frame

and Q is the ω mass minus the sum of the three pion masses.[7] The expected

λ distribution for the decay of a 1^- meson into three pions is also shown

in Fig. 2b. The events in the ω mass region fit the distribution well with

background included and disagree with the distribution in the neighboring

regions. No evidence for $N^*(1236)$ or $K^*(890)$ is observed in the events

lying in the ω mass region.

The invariant mass distributions of the two $K^+ K^-$ combinations in the

reaction $K^+ p \to K^+ p K^+ K^-$ are shown in Fig. 3 for both incident momenta.

A clear production of $\varphi \to K^+ K^-$ is observed in the mass region 1000 to

1040 MeV.

In Figs. 4 and 5 the Dalitz plots, $M^2(p\omega)$ vs $M^2(K^+\omega)$, are shown for the 188 $K^+\omega p$ events at 4.6 GeV/c and the 437 $K^+\omega p$ events at 9 GeV/c. The ω mass region is selected as 760 MeV $< M(\pi^+\pi^-\pi^0) <$ 820 MeV. In Figs. 6 and 7 are shown the invariant mass histograms $M(K^+\omega)$, $M(p\omega)$ and $M(K^+p)$ at both momenta. There is no evidence for the production of any narrow resonances in the $K^+\omega$ system. However, as seen from the Dalitz plot of the 9-GeV/c data (Fig. 4), the events tend to accumulate in the low $M^2(K^+\omega)$ and $M^2(p\omega)$ regions. The production center-of-mass angular distributions for the K^+, p and ω are shown in Figs. 8 and 9 and their four-momentum transfers squared in Figs. 10 and 11. In the 9-GeV/c data a strong forward peak is observed for the K^+-mesons while the proton peak is strongly backward. This suggests a peripheral production mechanism. These peripheral features are also seen in the 4.6-GeV/c data but they are much less pronounced at this lower momentum.

In Fig. 12 the Dalitz plot $M^2(p\varphi)$ vs $M^2(K^+\varphi)$ is shown for the 48 $K\varphi p$ events at 9 GeV/c. As in the case of the $K\omega p$ events no obvious resonance production is seen in the $K\varphi$ system, although a general accumulation of events is seen in the low $K\varphi$ mass region. At 4.6 GeV/c only 21 events fitted the hypothesis $K^+p \rightarrow K\varphi p$.

The clear peripheral nature of the $K^+\omega p$ data at 9 GeV/c and the absence of any noticeable resonance production strongly suggest the application of the multiperipheral Regge model. Because the higher energy data satisfy the criteria for the validity of this model better, we have attempted the analysis first on the 9-GeV/c data, and only these results are presented here. The applicability of the model at 4.6 GeV/c is discussed in Sec. V.

III.   THE DOUBLE-REGGE MODEL

We start the double-Regge analysis of the processes $K^+ p \to K^+ \omega p$ by drawing six diagrams of the type of Fig. 13 which differ from each other by permutations of the three final state particles. Each diagram defines a complete set of variables:

$$t_a = (p_3 - p_1)^2$$

$$t_b = (p_5 - p_2)^2$$

$$s_a = (p_3 + p_4)^2$$

$$s_b = (p_4 + p_5)^2$$

$$\cos \delta = \frac{(\tilde{p}_1 \times \tilde{p}_3) \cdot (\tilde{p}_2 \times \tilde{p}_5)}{|\tilde{p}_1 \times \tilde{p}_3| \cdot |\tilde{p}_2 \times \tilde{p}_5|} \quad . \tag{6}$$

Here $\tilde{p}_i$ denotes the three momentum of the particle labeled by i in the rest frame of particle 4. The contribution of each diagram to the amplitude is of the form[2]

$$A(s_a s_b t_a t_b \delta)\Big|_{\substack{t_a, t_b, \delta \text{ fixed} \\ s_a, s_b \text{ large}}} = \beta_a(t_a) R_a(s_a, t_a) \beta_I(t_a, \delta, t_b) R_b(s_b, t_b) \beta_b(t_b) \quad . \tag{7}$$

$R_a(s_a, t_a)$ is an expression having the Regge asymptotic behavior and phase

$$R_a(s_a, t_a)\Big|_{\substack{s_a \to \infty \\ t_a \text{ fixed}}} \sim \left(\frac{s_a}{s_o}\right)^{\alpha_a(t_a)} \sigma_a \exp[-\frac{i\pi}{2} \alpha_a(t_a)] \tag{8}$$

where α_a is a Regge trajectory with the quantum numbers defined by the corresponding diagram, and s_o is a constant introduced for dimensional reasons. We choose $s_o = 1$ GeV^2 in the conventional way. The quantity σ_a is either

+1 or +i according to whether the signature of the trajectory is even or odd.
Of course, this asymptotic behavior does not define R_a uniquely. The choice
of the optimum Regge representation for extrapolation to lower energies is
still an unsettled question, and we use that of Eq. (8) in the present analysis.

The real residue functions $\beta_a(t_a)$ and $\beta_b(t_b)$ are the same that appear in
two-body Regge analysis and we choose for them the standard exponential
parametrization

$$\beta(t) \sim e^{at} , \quad a = \text{constant} \tag{9}$$

which inhibits large values of the momentum transfer. It will be shown below
that in one case we need a zero in an external residue at $t \approx 0$. A similar
introduction of zeros has been found necessary in some two-body processes.[8]

The final element in Eq. (8) is the internal residue $\beta_I(t_a,\delta,t_b)$. We
expect this residue to decrease with increasingly negative values of t_a and
t_b for two reasons: (1) when t_a is continued analytically to the mass squared
of a particle lying on the Regge trajectory, this residue becomes an external
residue which decreases with increasing $-t_b$; (2) the integral of $|\beta|^2$ is
bounded by unitarity.[9] Thus we also assume that β is exponentially decreasing
in $-t_a$ and $-t_b$. The δ dependence of the internal residue is still unknown
except in some particular models,[10] and we will assume it to be negligible
in the present analysis. Therefore we use the parametrization:

$$A = K \exp[\frac{1}{2}(\gamma_a t_a + \gamma_b t_b)](\frac{s_a}{s_o})^{\alpha_a(t_a)} (\frac{s_b}{s_o})^{\alpha_b(t_b)} \sigma_a \sigma_b \exp[-\frac{i\pi}{2}(\alpha_a(t_a) + \alpha_b(t_b))] .$$
$$\tag{10}$$

Here K is determined by normalizing to the number of events, and γ_a and γ_b
incorporate the dependence on t_a and t_b due to both the internal and the

external vertices. For $\alpha(t)$ we choose straight lines with the following cri-

teria: if the trajectory is associated with a particle of mass m and spin J,

we require $\alpha(m^2) = J$ and $d\alpha/dt = 1/\text{GeV}^2$; for the Pomeranchuk trajectory

we set $\alpha(0) = 1$ and we take a small value for the slope ($d\alpha/dt = 0.12$).

Thus if $\alpha(t)$ is written as $\alpha_o + \alpha' t$ we use the values for α_o and α' as

given in Table I for the various possible exchanged trajectories. Note that

when α is a linear function of t, the parameters γ_a, γ_b and s_o in Eq. (10)

are not independent. Indeed, A depends only on the combinations $\frac{1}{2}\gamma_a - \alpha'_a \ell n\, s_o$

and $\frac{1}{2}\gamma_b - \alpha'_b \ell n\, s_o$.

It has been remarked by various authors that the contribution of different

multi-Regge graphs obtained by permutation of the final particles do not over-

lap, provided the momentum transfers are small and the subenergies are large.[2,11]

In our case, however, the problem of separating the different contributions

is a more delicate one, because we do not perform cuts in the subenergies.

The general approach is to include all six possible diagrams and divide the

available phase space into six different parts, retaining only the dominant

diagram in each region. After the events are fitted by separate contributions

of the dominant amplitudes, and thus the parameters in the amplitudes are

determined, the possibility of interferences among different diagrams should

be considered. However the problem is a circular one, because prior to the

determination of the parameters, the relative importance of two diagrams in

a region may not be clear. The problem may be solved by iteration and as

a first approximation we adopt the following procedure: each diagram defines

a different pair of invariant momentum transfers t_a and t_b and it peaks at

low values of $|t_a + t_b|$; thus we classify the events into six categories,

depending on which of the six possible $|t_a + t_b|$ combinations is minimum.

IV. APPLICATION TO THE $K^+\omega p$ DATA AT 9 GeV/c

When the above classification is applied, the 437 $K^+\omega p$ events fall into

different categories in the amounts shown in Fig. 13b. Note that the two

most populated categories do not involve baryon exchange, while the remaining

four do. Because too few events fall into all but the first two categories,

we attempt to fit only the latter.

Although the events involving baryon exchange are easily separated from

the two classes of events involving only meson and possibly Pomeranchuk

exchange (I and II in Fig. 13b), there is still some overlap between these

two classes. A plot of t_{KK} vs $t_{K\omega}$ for these (184 + 112 =) 296 events (Fig.

14) shows a concentration of events in the region where both t_{KK} and $t_{K\omega}$ are

small and close to each other. In view of this overlap we adopt the following

iterative procedure: first we divide the events into the two classes of 184

and 112 events and try to fit each diagram separately ignoring the overlap

in order to obtain initial values for the two residue parameters γ_a and γ_b

[see Eq. (10)]. Then we consider all 296 events together and add the results

of both diagrams, including the effects of interference terms.

First we consider the 112 events associated with diagram II in Fig. 13b.

Since strangeness exchange is involved in this case the number of possible

exchange pairs is small. Four exchange pairs seem plausible: K or K^* at

the meson vertex together with P or P' ($\equiv f_0$) at the nucleon vertex. The

procedure in each case is to choose values of γ_a and γ_b [see Eq. (10)], which

for this diagram are $\gamma_{K\omega}$ and γ_{pp}, and to generate phase space events by Monte

Carlo calculation on a computer, and weight them by the modulus square of the

matrix element given by Eq. (10). This calculational technique enables us

to perform cuts on the theoretical distribution in any kinematical quantity

and to plot all kinematical quantities with ease. To calculate these distri-
butions from explicit analytical expressions or by numerical methods tends
to be more difficult in general. The same cut performed on the data, i.e.,
that $|t_{K\omega} + t_{pp}|$ be minimum is applied to the theoretical calculation. Using
the values of $\gamma_{K\omega}$ and γ_{pp} which best reproduce the experimental distributions
in $t_{K\omega}$ and t_{pp} we compare the theory with the distributions in the production
center-of-mass angle of the "interior" particle, here the K^+, in the three
possible mass combinations, and on the Dalitz plot. There is one difficulty
with this diagram before we can proceed, and that is that the experimental
distribution in $t_{K\omega}$ peaks at 0.4 $(GeV/c)^2$ and falls rapidly towards $t_{K\omega} = 0$.
In order to reproduce this behavior we have to put a zero into the amplitude
at $t_{K\omega} = 0$. Similar zeros have been introduced into Regge residues in existing
analysis of two-body data.[8] This is done by modifying Eq. (10) slightly so
that the contribution to the amplitude from the residue function at the meson
vertex has an extra factor of $-t_{K\omega}$. With this change in the amplitude the
calculation was done according to Eq. (10) and the results are shown in Figs.
15 through 18. Figure 15 shows the experimental distributions in $t_{K\omega}$ and t_{pp},
with the smooth curves showing the results of the best values of $\gamma_{K\omega} = 1.0$
$(GeV/c)^{-2}$, $\gamma_{pp} = 4.0$ $(GeV/c)^{-2}$ for the exchange pair (K, P) and $\gamma_{K\omega} = 1.0$
$(GeV/c)^2$, $\gamma_{pp} = 2.0$ $(GeV/c)^2$ for the exchange pair $(K^*(890),P')$. We do not
consider the exchange pair (K^*, P) because of Morrison's selection rule.[12]
The exchange pair (K, P') gives results intermediate between the two cases
presented here. Note that to fit the data a larger value for γ_{pp} is needed
if there is a Pomeranchuk at the nucleon vertex than if there is a P' at the
nucleon vertex. This is due to the smaller slope in t of the Pomeranchuk
trajectory (see Table I). Figure 16 shows the production center-of-mass

distribution of the "interior" particle, here the K^+, and again the smooth
curves show the result of the calculations for the two exchange pairs. The
(K^*, P') exchange gives a better fit than the (K, P) exchange. Figure 17
shows the three mass distributions and we note that the (K, P) exchange pair
is especially poor in the (K^+p) mass distribution, while the (K^*, P') exchange
pair fits all three mass distributions reasonably well. Figure 18 shows the
Dalitz plot $M^2(K\omega)$ vs $M^2(Kp)$ for these events. A rough measure of the good-
ness of fit on the two-dimensional Dalitz plot is given by calculating the
distribution in the quantity $x_K = \ell n \, (s_{K\omega}/s_{Kp})$. The line $x_K = 0$ divides
the Dalitz plot along a 45° line. The real events have 84 events with x
negative and 27 with x positive or 24% with x positive. The (K^*, P') exchange
pair predicts 23% positive, while the (K, P) exchange pair predicts only 7%
positive. Thus we conclude that the (K^*, P') exchange pair fits the data
with $|t_{K\omega} + t_{pp}|$ minimum best. If we adopt the point of view of trying to
fit the data using the least number of diagrams, then we can say that there does
not appear to be any strong need for Pomeranchuk exchange for these events.

We next consider the 184 events associated with diagram I of Fig. 13b.
In this case there is neither strangeness exchange nor baryon exchange and
so the number of plausible exchange pairs is larger. We consider only two
cases: (1) (ω, P) and (2) (ω, P'). Note that in considering the (ω, P')
exchange pair, for example, there is a priori no reason to put the ω at the
meson vertex and the P' at the nucleon vertex; the reverse is just as plausible.
In fact, both diagrams must be considered along with the interference term
between them. In average the subenergy associated with Pomeranchuk exchange
is larger than that with meson exchange, and therefore the diagrams with (P, ω)
and (ω, P) exchange pairs tend to populate different regions of the Dalitz

plot. The ratio of the two amplitudes was estimated by normalizing each amplitude in the region of the Dalitz plot where it dominates, to the observed number of events in that region. This ratio is

$$\frac{K^2(\omega,P)}{K^2(P,\omega)} = 0.79, \tag{11}$$

where the K's are defined in Eq. (10). On the other hand, since the ω and P' have similar trajectories, addition of the (P', ω) exchange pair to the (ω, P') exchange pair does not modify the results. Thus, for these 184 events we consider two cases. Case I involves (ω, P) and (P, ω) exchange pairs, and Case II involves (ω, P') exchange. The results are shown in Figs. 19 through 22. Figure 19 shows the experimental distributions in t_{KK} and t_{pp}, with the smooth curves referring to Cases I and II above. The best fit values of γ's used are $\gamma_{KK} = \gamma_{pp} = 2.0$ $(GeV/c)^{-2}$ for Case I and $\gamma_{KK} = \gamma_{pp} = 0.0$ $(GeV/c)^{-2}$ for Case II. Figure 20 shows the production center-of-mass angular distribution for the "interior" particle, here the ω meson. Neither exchange pair adequately explains the forward ω peak: this will be discussed in detail in the next section which deals with the combined (112 + 184) non-baryon-exchange sample. Figure 21 shows the three mass distributions for these events and no discrimination between the two exchange pairs (ω, P) and (ω, P') can be made. Figure 22 shows the Dalitz plot for these events. The distribution in the quantity $x_\omega = \ell n\ (s_{K\omega}/s_{\omega p})$ has been calculated and the agreement with the data has been found to be satisfactory.

We next consider the combined sample of 296 events with either $|t_{KK} + t_{pp}|$ or $|t_{K\omega} + t_{pp}|$ minimum. The calculation of the diagram with the K^+ as the "interior" particle (112 events) and with (K^*, P') exchange pair using the best values of $\gamma_{K\omega}$ and γ_{pp} shows that 45% of the intensity of this diagram

is lost by the requirement that $\left| t_{K\omega} + t_{pp} \right| < \left| t_{KK} + t_{pp} \right|$. For the events
with the ω as the "interior" particle and with the two diagrams with (ω, P)
exchange pair the loss due to the cut $\left| t_{KK} + t_{pp} \right| < \left| t_{K\omega} + t_{pp} \right|$ is 6%. The
sharp forward peak in the angular distribution of the ω for the 184 events
is due partially to contamination from events which should have been classed
with the 112 events with the K^+ as the "interior" particle, as discussed
earlier. According to our stated procedure we now use the parameters deter-
mined for the separate fits to the 112 and 184 events to fit the 296-event
combined sample.

The amplitude for each diagram is given by Eq. (10), and the three diagrams
we use are: (1) the ω is the "interior" particle and the exchange pair is ω
at the meson vertex and Pomeranchuk at the baryon vertex; (2) the ω is the
"interior" particle and the exchange pair is Pomeranchuk at the meson vertex
and ω at the baryon vertex; and (3) the K^+ meson is the "interior" particle
and the exchange pair is $K^*(890)$ at the meson vertex and P' at the baryon
vertex. The relative strengths of the three diagrams are determined by Eq.
(11) and by the normalization

$$\frac{\int \left| A_1 + A_2 \right|^2 d\varphi}{\int \left| A_3 \right|^2 d\varphi} = \frac{184}{112} \quad , \qquad (12)$$

in which $\int \left| A_i \right|^2 d\varphi$ means the integral over phase space of a particular matrix
element with the proper cut in $\left| t_a + t_b \right|$. The values of K used in the fit
are $K_1 = 0.04$, $K_2 = 0.07$, and $K_3 = 1.0$ where the modulus squared of the
matrix element used is $\left| A \right|^2 = \left| A_1 + A_2 + A_3 \right|^2$. We have considered the
possibility of a ratio of the K's to be negative and have found the results
to be less satisfactory. The results are shown in Figs. 23 through 26.

Figure 23 shows the three t-distributions t_{KK}, t_{pp} and $t_{K\omega}$; Fig. 24 shows the

three production center-of-mass angular distributions; Fig. 25 shows the three

invariant mass distributions; and Fig. 26 shows the Dalitz plot. In all instances

agreement between theory and experiment is good. We emphasize that the separate

fits to the 112 and 184 event subsamples with $|t_{K\omega} + t_{pp}|$ and $|t_{KK} + t_{pp}|$

minimum, respectively, are not to be taken too seriously, due to the large overlap

between these two diagrams. We have used them as an intermediate step to

obtain approximate parameters and ratios for the various diagrams. We further

emphasize that we have succeeded in fitting the entire Dalitz plot for the

$K^+\omega p$ events with no cuts in the subenergies and a cut in the four-momentum

transfers which essentially only eliminates baryon exchange. For summary of

the parameters used in this fit, see Table II.

V. DISCUSSION AND CONCLUSIONS

In the present work we are primarily interested in studying the extent

to which the multi-Regge model is able to successfully describe reaction

processes. To this end we selected the reaction $K^+p \to K^+\omega p$ at 9 GeV/c

where no strong resonances are observed, since the Regge model is not expected

to reproduce resonance effects in detail. In addition, we show that in this

case we do not need to introduce any cuts in the subenergies, and have the

possibility of fitting the entire sample of events on the complete Dalitz

plot. Our approach is thus consistent with previous analyses where low mass

resonances were excluded by cuts on the Dalitz plot.[2-5] Furthermore, we

expect that the background events in the ω mass region ($\sim 35\%$) modify very

little, if at all, the characteristics of the various mass and angular distri-

butions. This conclusion was deduced from the experimental observation that

the various mass and angular distributions for the neighboring $M(\pi^+\pi^-\pi^0)$ regions

$(640 < M(\pi^+\pi^-\pi^0) < 760$ MeV and $820 < M(\pi^+\pi^-\pi^0) < 940$ MeV$)$ are very similar

to the corresponding ones in the ω region apart from the expected difference

in the λ distributions.

We adopted in this work the criterion of $|t_a + t_b|$ = minimum for the

classification of the events into the six double-Regge diagrams where we

encountered difficulties due to the overlapping of the various double-Regge-

matrix-element contributions in the Dalitz plot. Previous analyses have

adopted classification methods based on the hierarchy of the longitudinal

momenta of the three final-state particles $(P_{L1} > P_{L2} > P_{L3})$. We have also

applied this last method to our data with the result that the total number

of events assigned to the diagrams I and II of Fig. 16b remained essentially

the same, but the internal division between these two diagrams was somewhat

different from the one obtained by the $|t_a + t_b|$ minimum criterion. The

longitudinal momentum criteria was found to suffer from the matrix elements

overlapping problem as well, and no obvious advantage has been found in using

one or the other method in this experiment.

In the double-Regge model analysis one can consider in principle all the

six diagrams at the same time. This leads, however, to numerous possible

variations of the exchange trajectories, residue functions and coupling

constants. Consequently, to obtain a more meaningful analysis, we have

restricted ourselves to the events assigned to the two most populated double-

Regge diagrams (diagrams I and II of Fig. 13b). In this way we are able to

describe successfully about 2/3 of the events with 1/3 of the possible diagrams.

There is no reason to doubt that the remaining 1/3 of the data may equally well

be fitted by the four diagrams III to VI of Fig. 13b. In addition, our fit

successfully describes the distributions in derived kinematical quantities

such as the Treiman-Yang angles. At this point, it should be stressed that

the choice of Regge trajectories used in this work is by no means the only

possible one to fit the data.

Due to the overlapping of the matrix elements, we expect some contamina-

tion in the fitted events from the diagrams that we have neglected (III to VI).

Such a contamination is likely to be responsible for the broadening of the t-

distributions (see Fig. 23) and for this reason in the fitting of the residue

parameters γ we have neglected the tail of the t-distribution.

No serious attempt has been made to apply the double-Regge model to the

$K^+p \rightarrow K^+\omega p$ data at 4.6 GeV/c since it seemed to us to be less meaningful

than at 9 GeV/c for the following reasons:

a) The validity of the Regge model is expected to decrease at lower incident

   momenta.

b) The problem of the overlapping of the various matrix elements is more severe

   at lower energies.

c) The number of events is relatively small; i.e., 188 at 4.6 GeV/c in comparison

   with 437 at 9 GeV/c.

Finally, it is interesting to observe that φ production in the reaction

$K^+p \rightarrow K^+\varphi p$ is smaller by a factor of 0.26±0.05 than ω production in the

reaction $K^+p \rightarrow K^+\omega p$. Since the φ and the ω are particle mixtures in the

SU(3) classification it is of considerable interest to compare a double-Regge

analysis of the φ production with that of the ω production. Unfortunately

the small number of φ events even at the 9-GeV/c data prohibits any meaningful

analysis at this time.

FOOTNOTES AND REFERENCES

*Work supported by the U. S. Atomic Energy Commission.

1. T. W. B. Kibble, Phys. Rev. 131, 2282 (1963); K. A. Ter-Martirosyan,

    Soviet Phys. JETP 17, 233 (1963).

2. Chan Hong-Mo, K. Kajantie and G. Ranft, Nuovo Cimento 49A, 157 (1967).

3. Chan Hong-Mo, K. Kajantie, G. Ranft, W. Beusch and E. Flaminio, Nuovo

    Cimento 51A, 696 (1967).

4. S. Ratti, Topical Conference on High Energy Collisions of Hadrons, CERN,

    Geneva, Vol. I, p. 611, January 1968.

5. E. Berger, Phys. Rev. 166, 1525 (1968).

6. R. Dolen, D. Horn, and C. Schmid, Phys. Rev. 166, 1768 (1968); G. F. Chew

    and A. Pignotti, Phys. Rev. Letters 20, 1078 (1968).

7. G. Goldhaber, S. Goldhaber, J. A. Kadyk, and B. C. Shen, Phys. Rev. Letters
    15, 118 (1965).

8. A zero in the ω residue was introduced by W. Rarita and V. L. Teplitz,

    to account for the crossover of the pp and $\bar{p}$p differential cross sections

    (see Phys. Rev. Letters 12, 206 (1964).) J. S. Ball, W. R. Frazer, and

    M. Jacob are also forced to introduce zeroes in the pion and kaon exchange

    contributions to pion and kaon photoproduction (see Phys. Rev. Letters 20,

    518 (1968).) We cannot rule out the possibility that the zero that we

    observe is due to interferences among different possible Regge exchanges

    in the same diagram.

9. I. A. Verdiev, O. V. Kancheli, S. G. Matinyan, A. M. Popova and K. A. Ter-

    Martirosyan, Soviet Physics JETP 19, 1148 (1964).

10. R. Blankenbecler and R. L. Sugar, Fenyman Diagram Models of Regge and

    Multi-Regge Couplings, University of California at Santa Barbara preprint.

11. F. Zachariasen and G. Zweig, Phys. Rev. 160, 1322 (1967).

12. D. R. O. Morrison, Phys. Rev. 165, 1699 (1968).

Table I.   Trajectory parameters.

Trajectory	α_0	α'
Pomeranchuk	1.0	0.12
K	- 0.25	1.0
$K^*(890)$	0.2	1.0
ω	0.387	1.0
P'	0.44	1.0

Table II. Summary of parameters.

	Criterion	Events	γ_a	γ_b	$\alpha_a(0)$	$\alpha_b(0)$	Fig. Nos.
(a)	$\lvert t_{K\omega} + t_{pp} \rvert$ minimum	112	1.0	2.0	0.2	0.44	18-21
(b)	$\lvert t_{KK} + t_{pp} \rvert$ minimum	184	2.0	2.0	0.387	1.0	22-25
			2.0	2.0	1.0	0.387	
	(a) or (b)	296	1.0	2.0	0.2	0.44	26-29
			2.0	2.0	0.387	1.0	
			2.0	2.0	1.0	0.387	
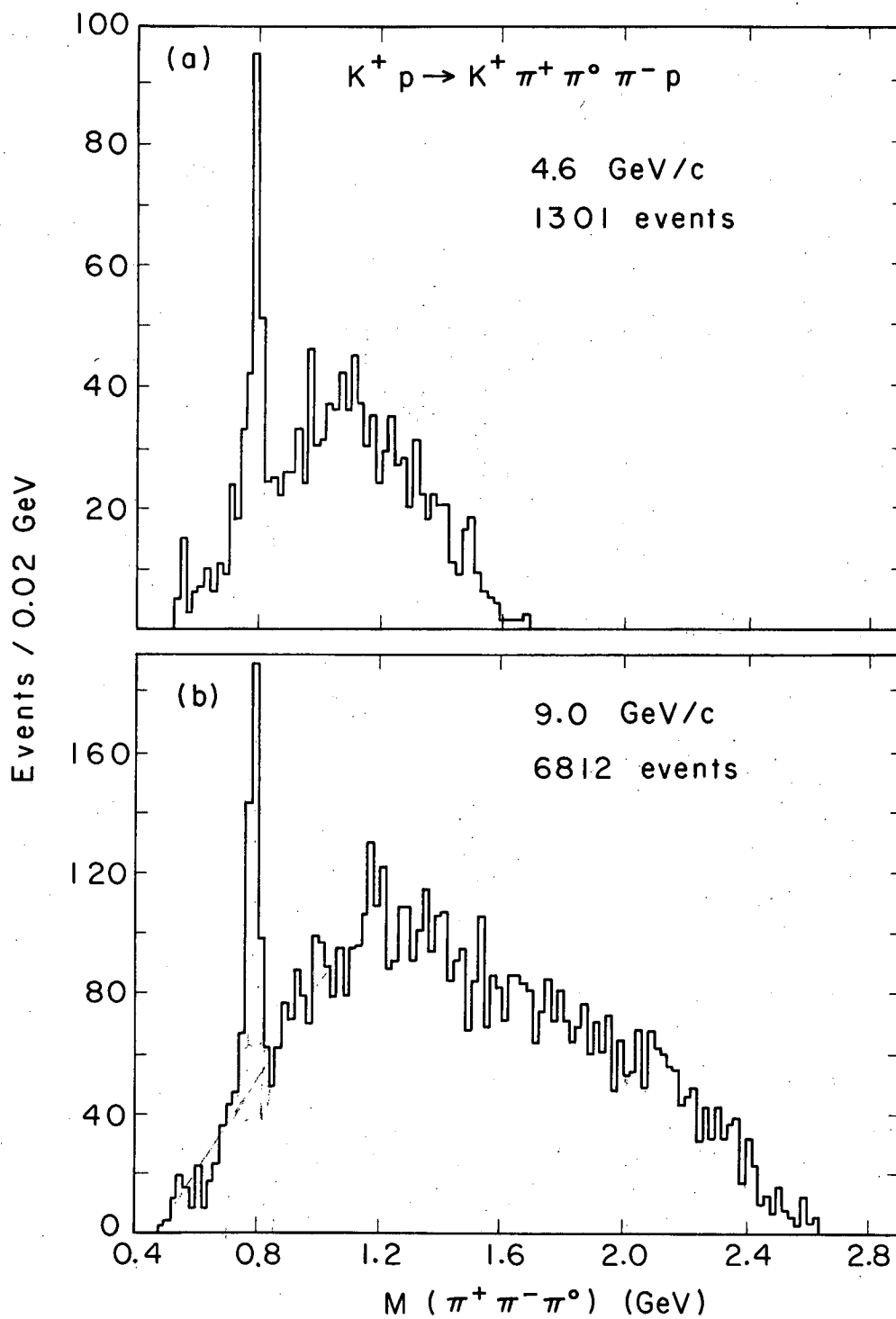
Fig. 1. Invariant mass distribution $M(\pi^+\pi^-\pi^0)$ for the reaction $K^+ p \to Kp\pi^+\pi^-\pi^0$ at (a) 4.6 GeV/c and (b) 9.0 GeV/c.
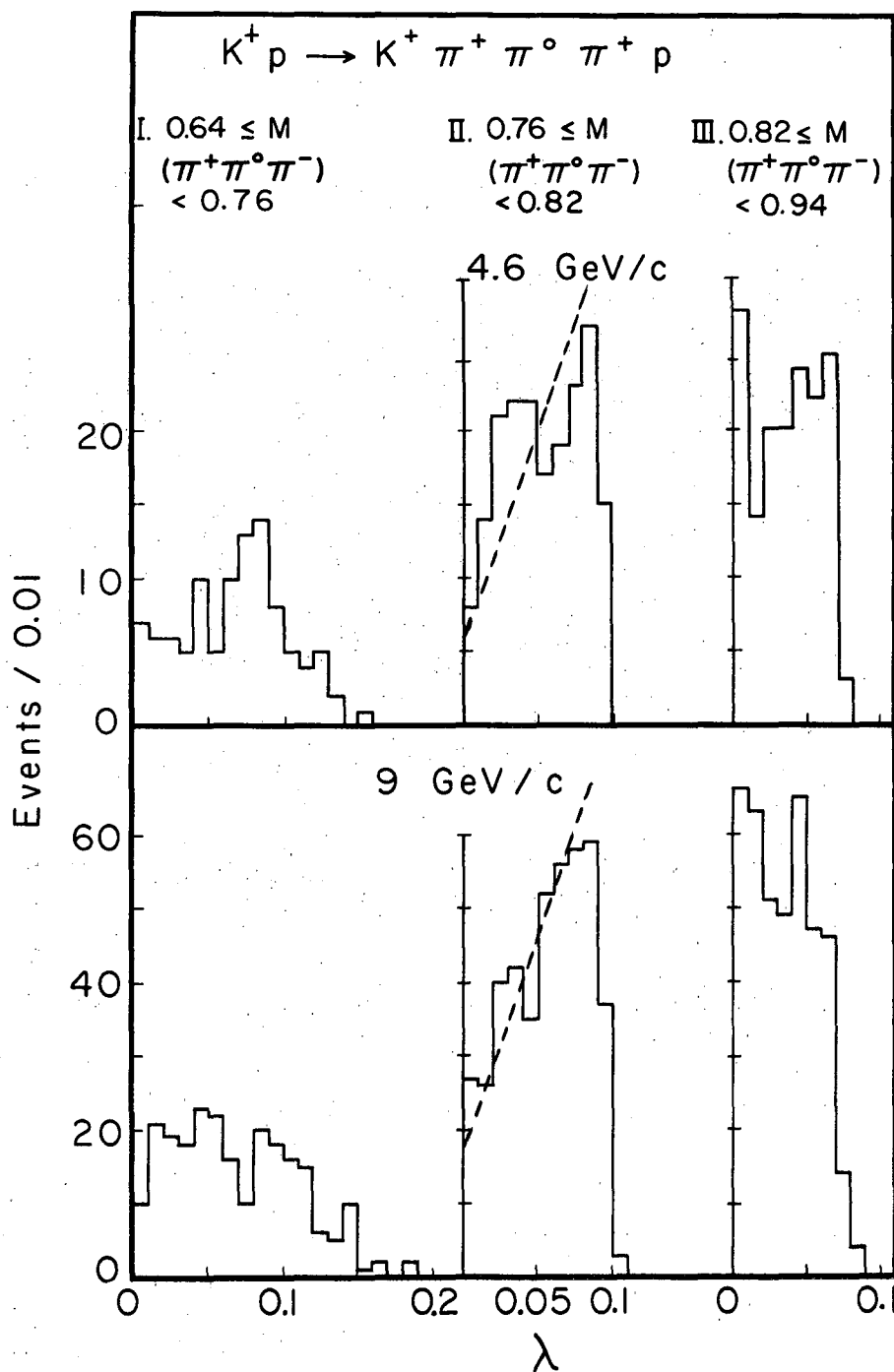
Fig. 2. Distributions of the λ parameter for the $\pi^+\pi^-\pi^0$ system at the ω mass and neighboring regions in the reaction $K^+p \rightarrow K^+\pi^+\pi^-\pi^0 p$ at 4.6 and 9.0 GeV/c. The dashed lines represent the expected distribution of a 1^- meson decay plus background.

(a) $K^+ p \rightarrow K^+ K^+ K^- p$

4.6 GeV/c

26 events; 2 comb./events

(b) 9.0 GeV/c

200 events; 2 comb./events

M ($K^+ K^-$) (GeV)

Events / 0.02 GeV
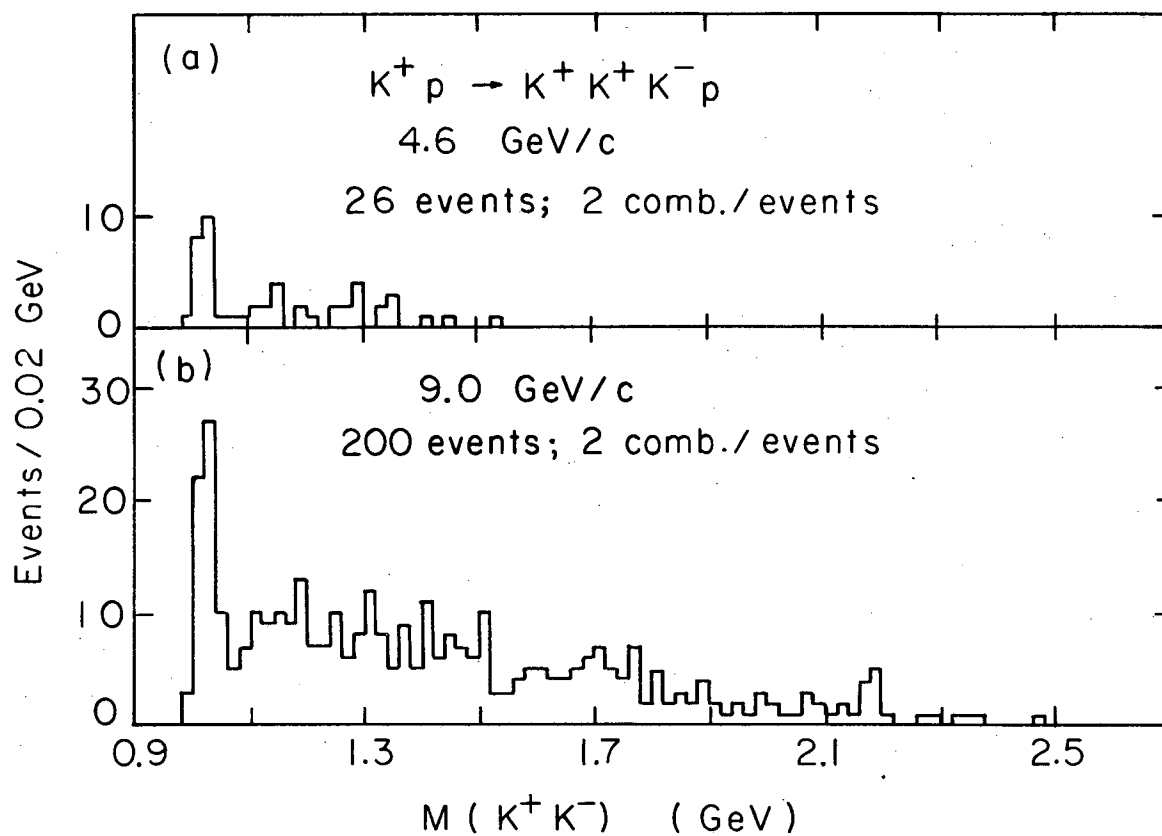
XBL687-3375

Fig. 3. $K^+ K^-$ invariant mass distribution in the reaction $K^+ p \rightarrow K^+ K^+ K^- p$ where each event is plotted twice; (a) at incident momentum of 4.6 GeV/c, and (b) at incident momentum of 9.0 GeV/c.
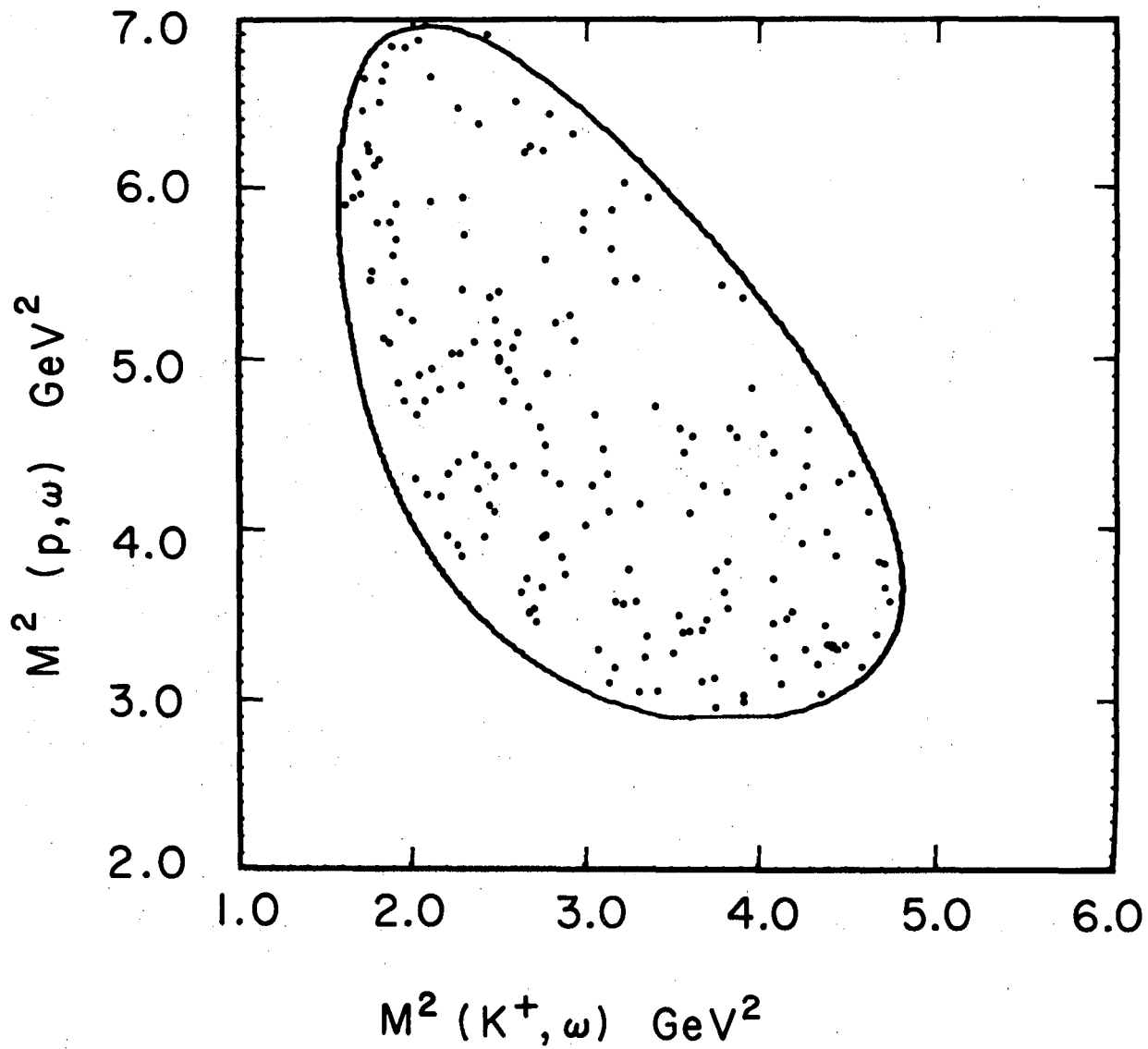
Fig. 4. The Dalitz plot of $M^2(p, \omega)$ vs $M^2(K^+, \omega)$ for the reaction $K^+ p \rightarrow K^+ \omega p$ at 4.6 GeV/c.

XBL687-3430

$K^+\omega p$

437 Events
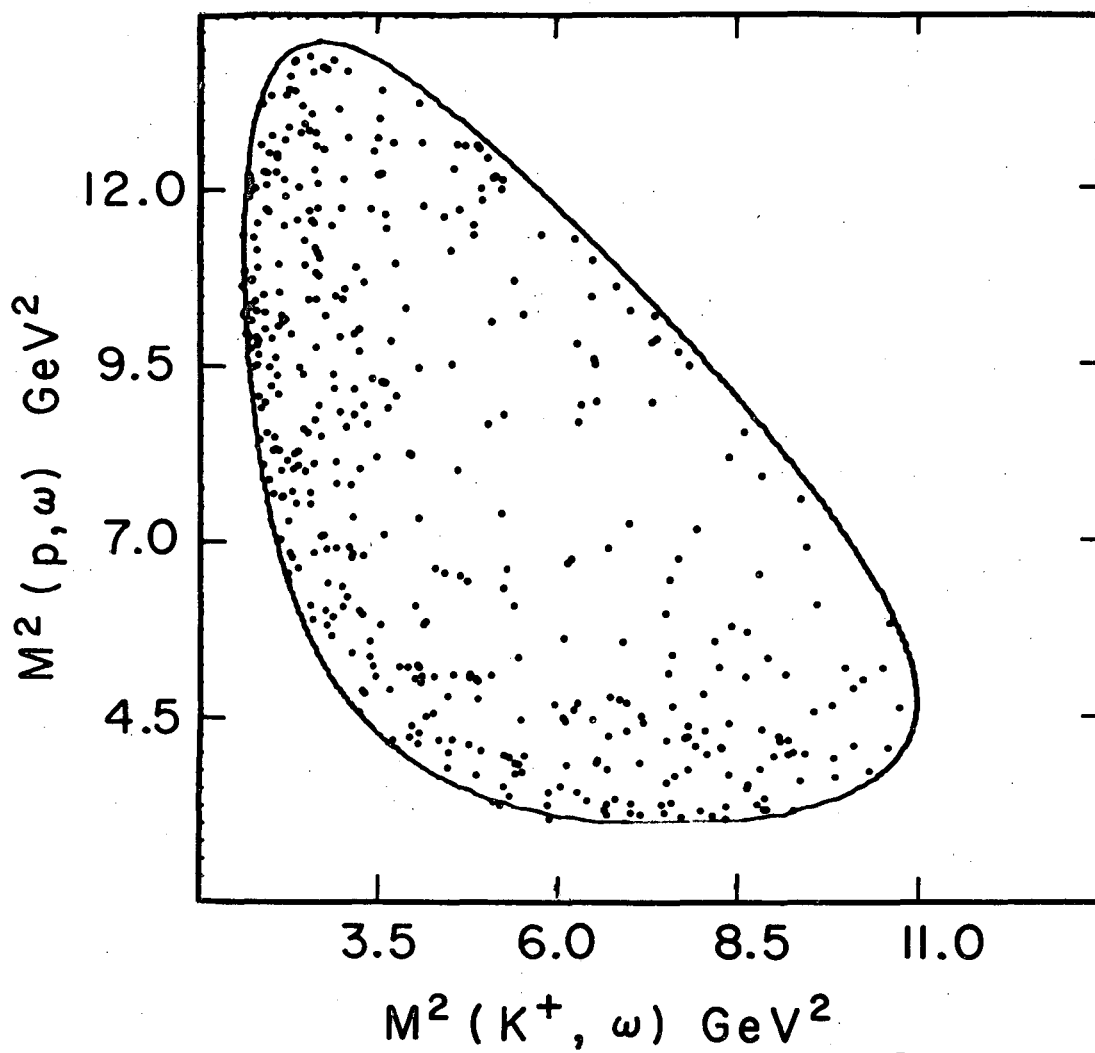
XBL687-3425

Fig. 5. The Dalitz plot of $M^2(p, \omega)$ vs $M^2(K^+, \omega)$ for the reaction $K^+p \rightarrow K^+\omega p$ at 9.0 GeV/c.
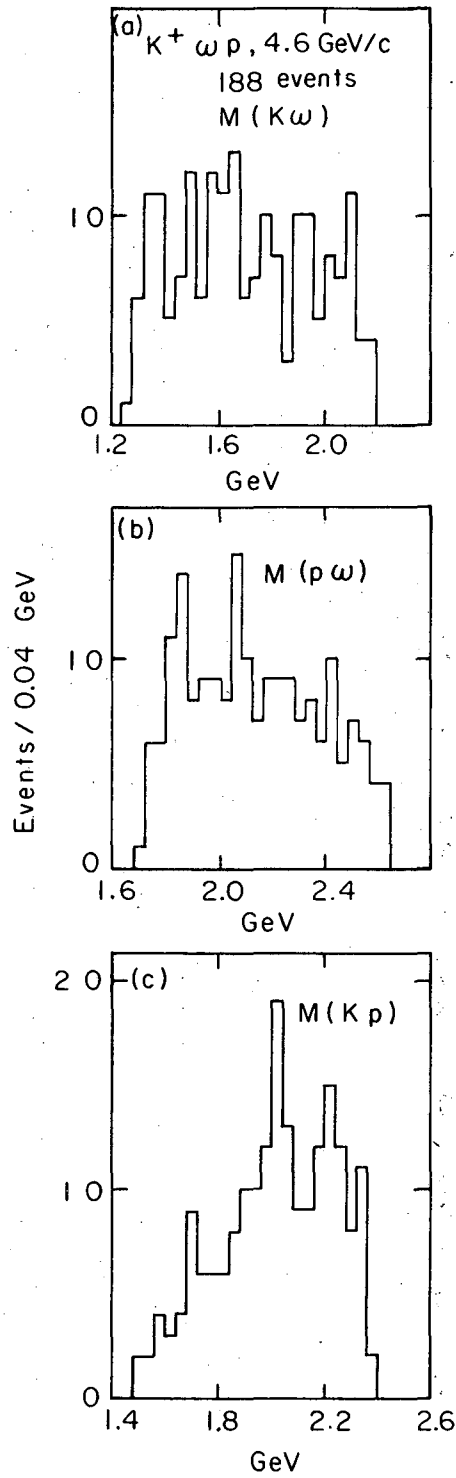
XBL687-3371

Fig. 6. Invariant mass distributions in the reaction $K^+p \to K^+\omega p$ at 4.6 GeV/c; (a) $M(K^+, \omega)$, (b) $M(p, \omega)$, and (c) $M(K^+, p)$.
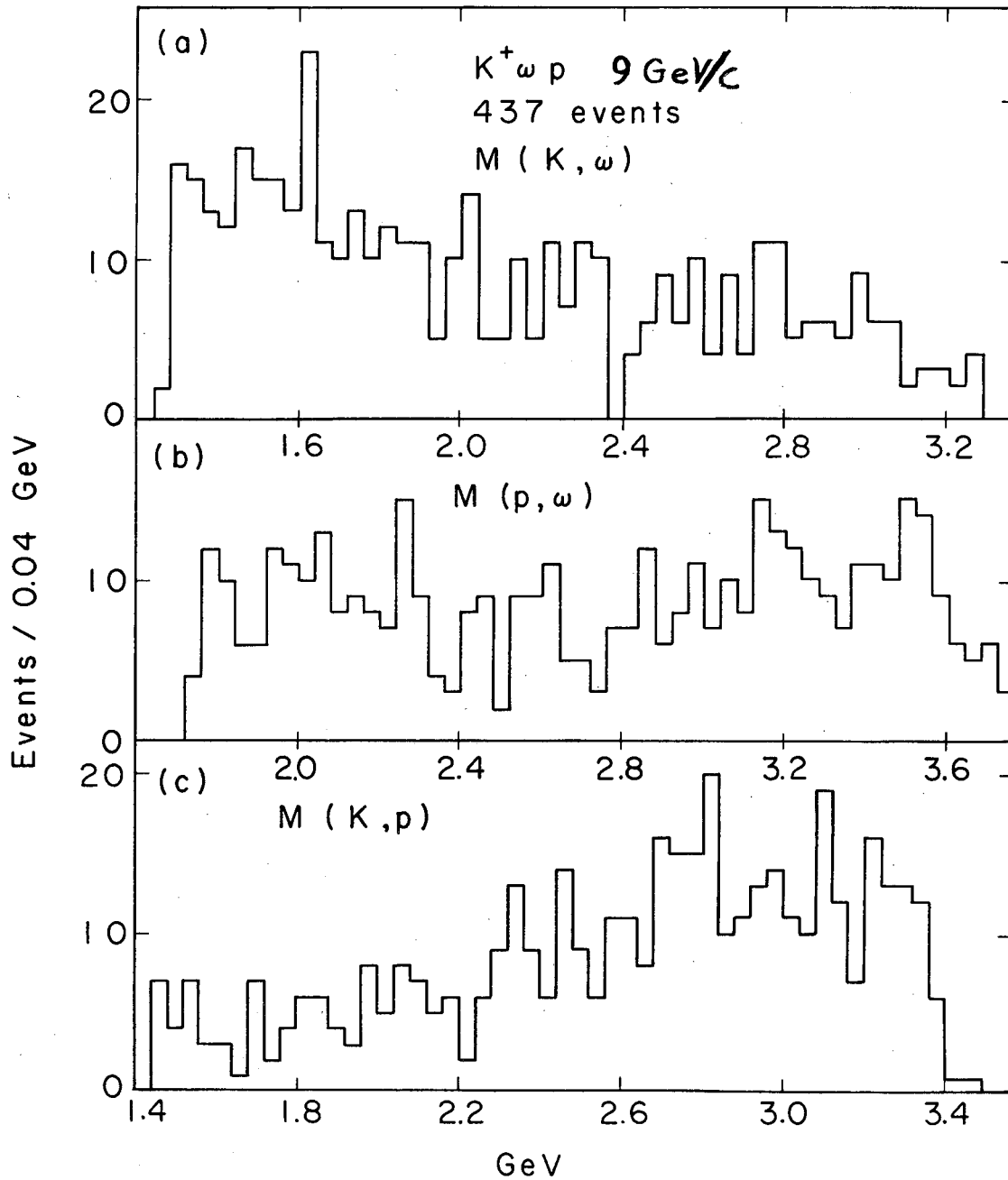
Fig. 7. Invariant mass distributions in the reaction $K^+p \to K^+\omega p$ at 9.0 GeV/c; (a) $M(K^+, \omega)$, (b) $M(p, \omega)$, and (c) $M(K^+, p)$.
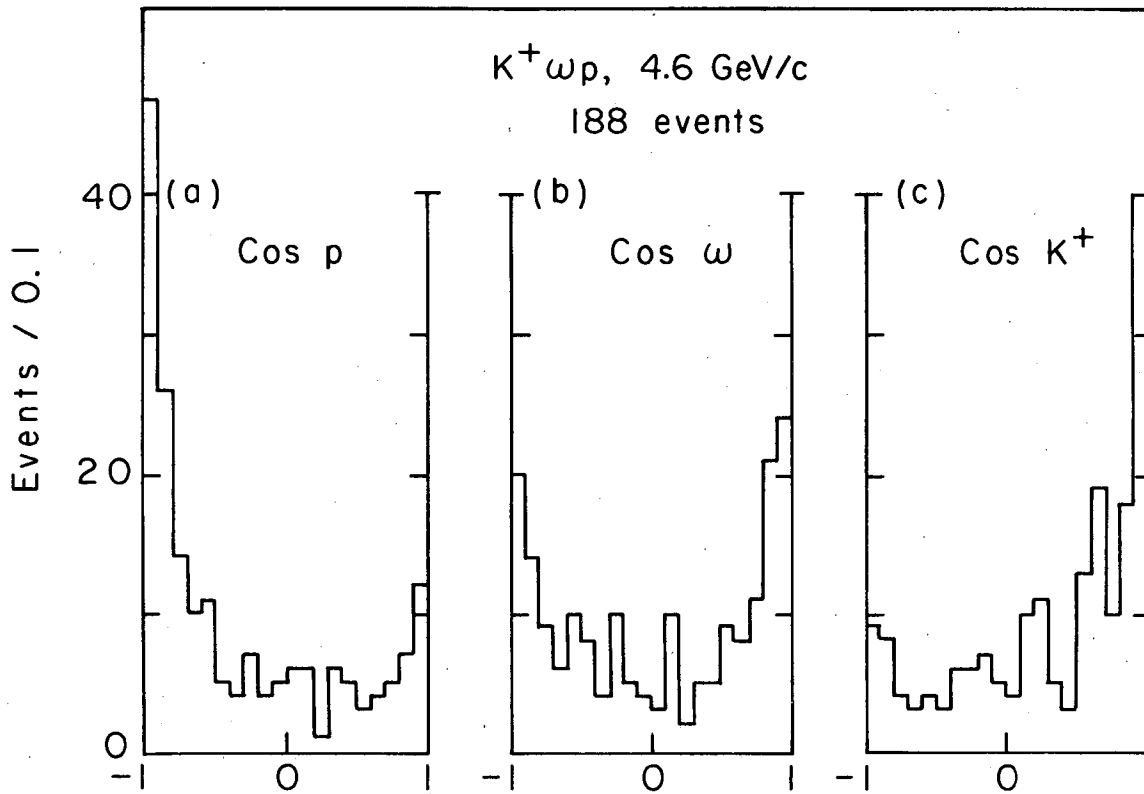
Fig. 8. Angular distribution in the production center of mass of the final

state particles in the reaction $K^+p \rightarrow K^+\omega p$ at 4.6 GeV/c; (a) $\cos \theta_p$,

(b) $\cos \theta_\omega$, and (c) $\cos \theta_{K^+}$.
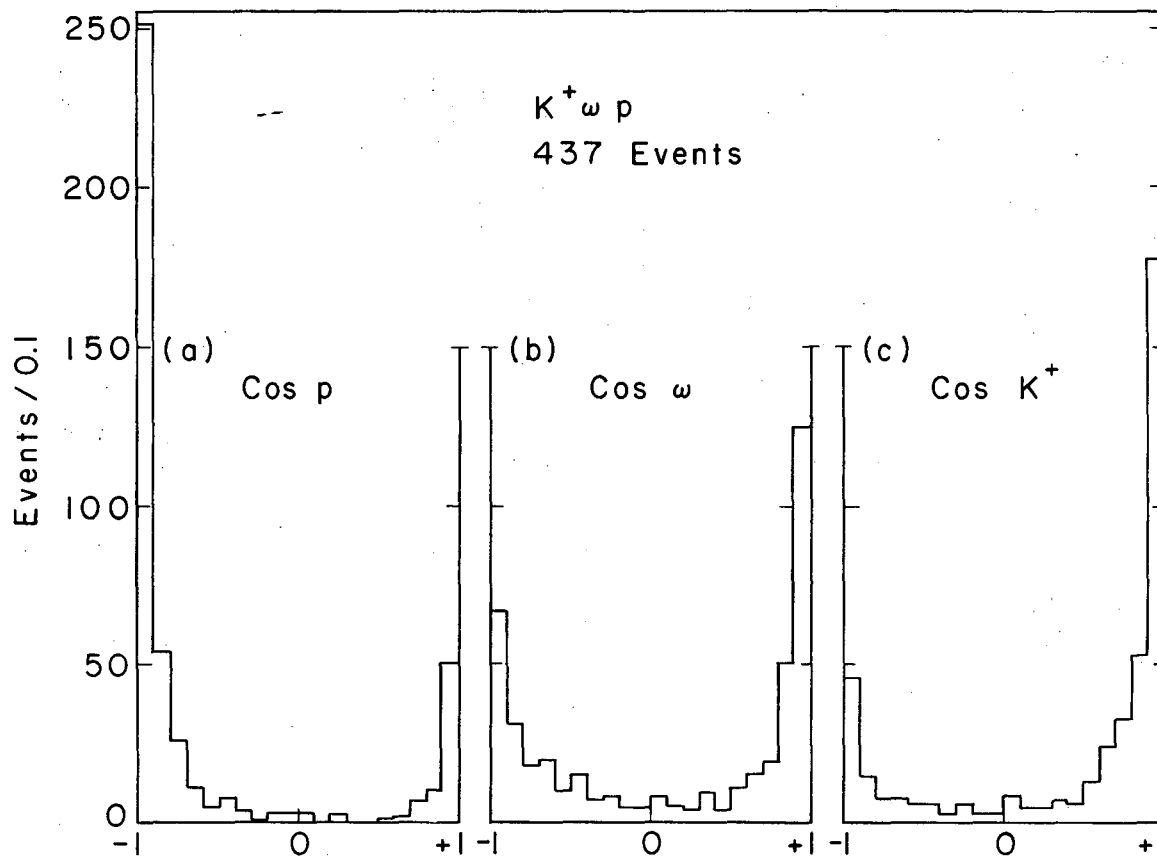
XBL687-3377

Fig. 9. Angular distribution in the production center of mass for the final

state particles in the reaction $K^+p \rightarrow K^+\omega p$ at 9.0 GeV/c; (a) cos θ_p,

(b) cos θ_ω, and (c) cos θ_{K^+}.
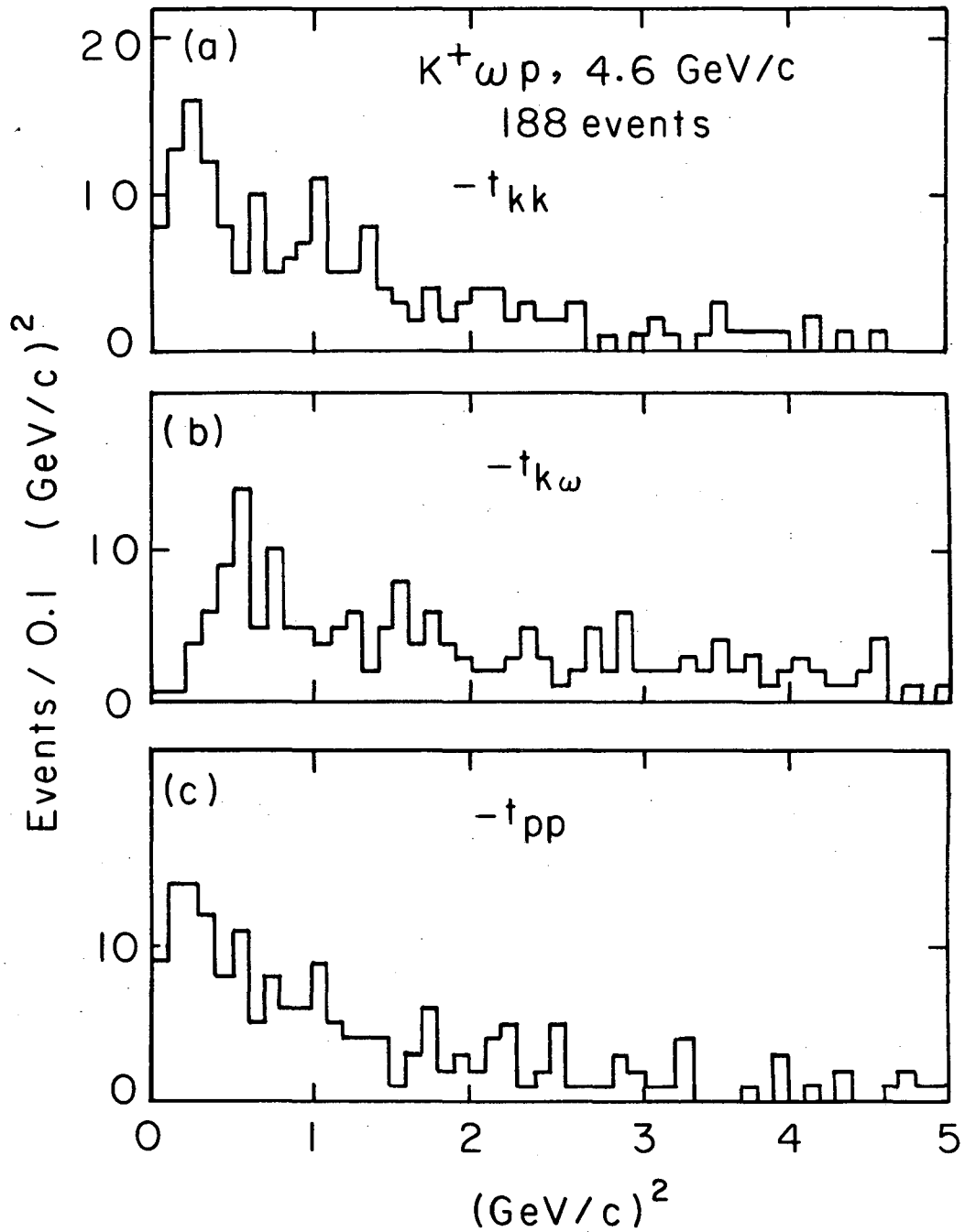
Fig. 10. Four momentum transfer distributions in the reaction $K^+p \to K^+\omega p$ at 4.6 GeV/c; (a) t_{KK}, (b) $t_{K\omega}$, and (c) t_{pp}.
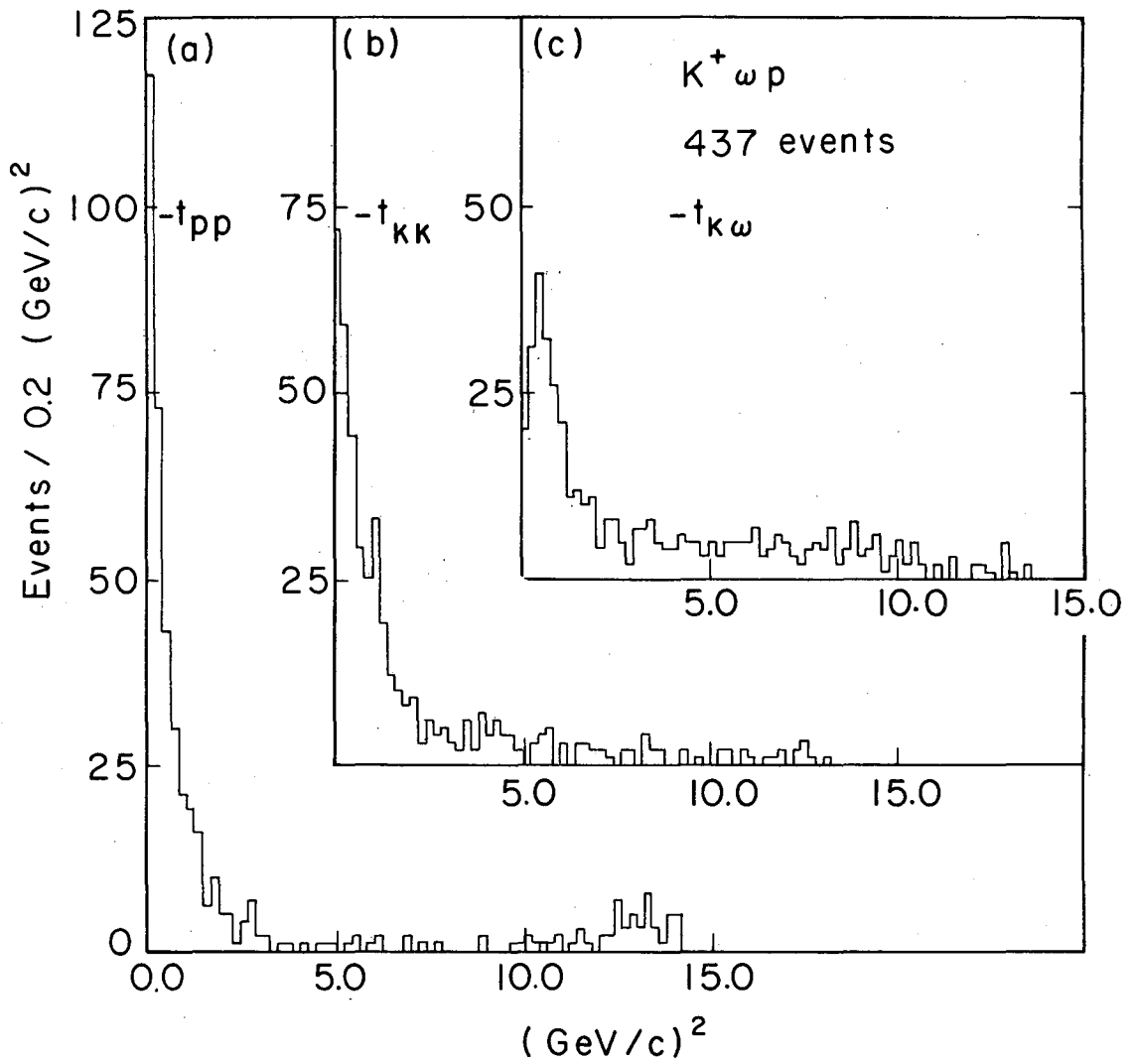
XBL687-3373

Fig. 11. Four momentum transfer distributions in the reaction $K^+p \to K^+\omega p$

at 9.0 GeV/c: (a) t_{pp}, (b) t_{KK}, and (c) $t_{K\omega}$.

$K^+ \phi p$

48 Events
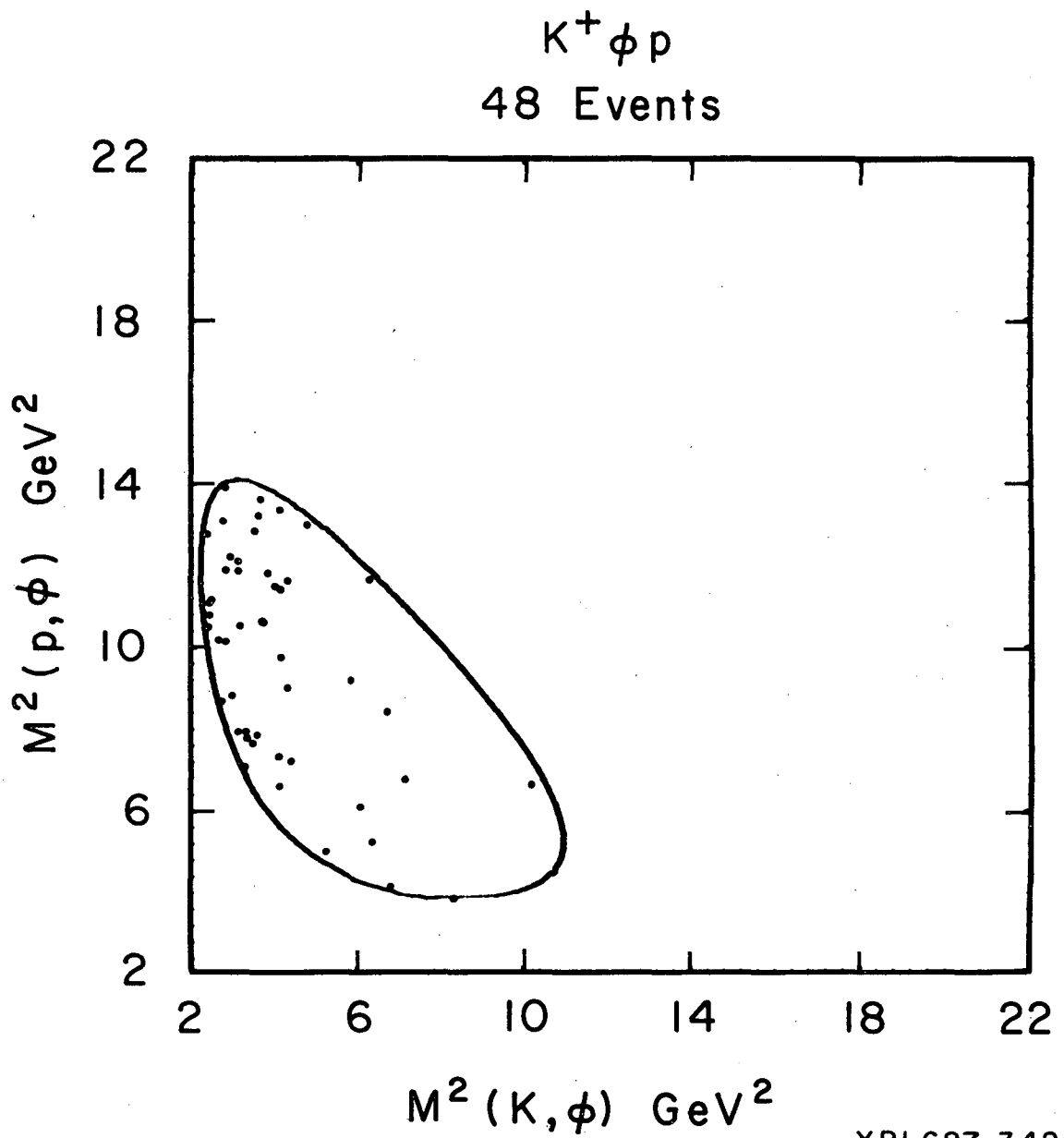
Fig. 12. The Dalitz plot of $M^2(p, \varphi)$ vs $M^2(K, \varphi)$ for the reaction $K^+ p \rightarrow K^+ \varphi p$ at 9.0 GeV/c.

XBL687-3429
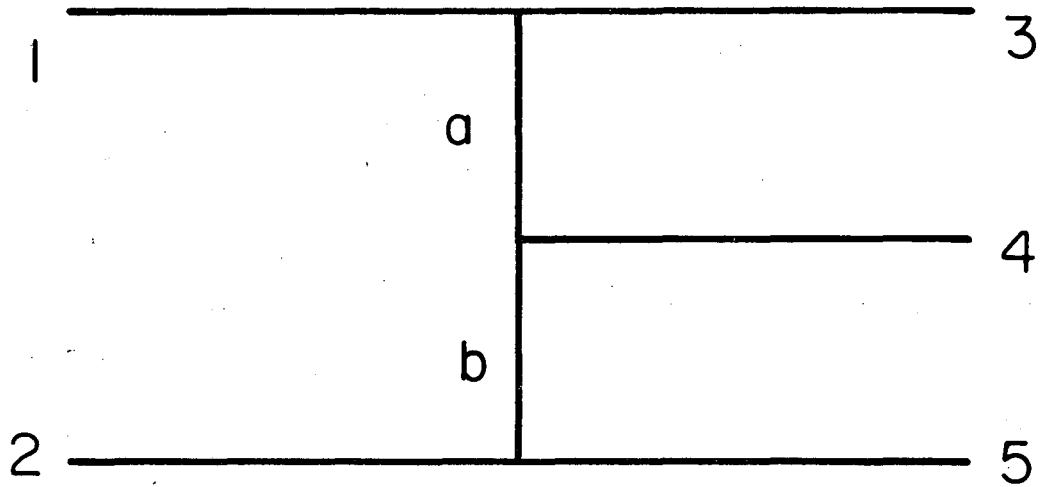
XBL687- 3367

Fig. 13. (a) Double peripheral diagram; (b) the six possible peripheral

diagrams for the reactions $K^+p \to K^+\omega p$ and $K^+p \to K^+\varphi p$. The numbers

on the side represent the number of $K^+p \to K\omega p$ events at 9.0 GeV/c

assigned to each diagram through the $|t_a + t_b|$ minimum criterion.

Fig. 13b.

XBL687-3370

$K^+ \omega p$

296 Events

XBL687-3424
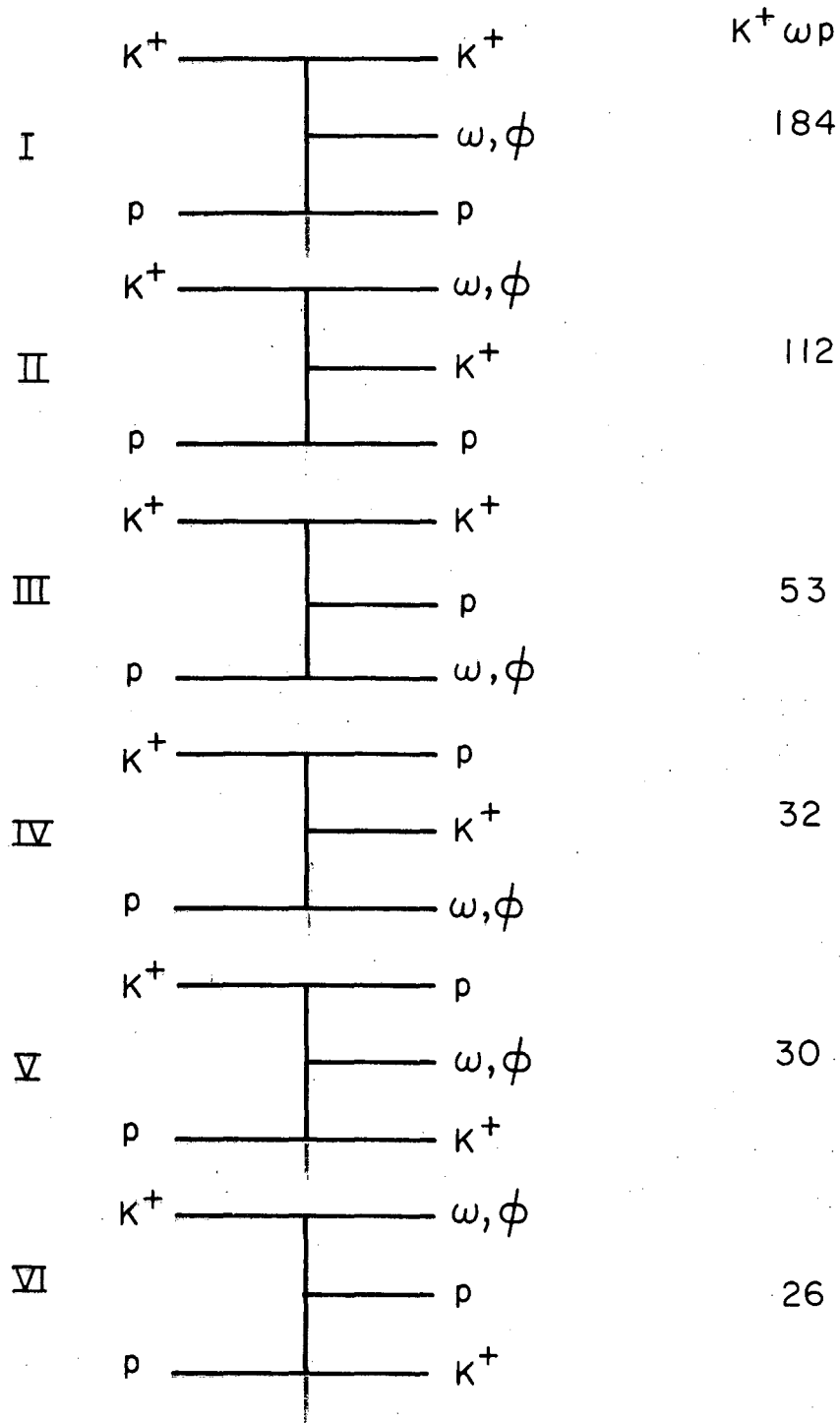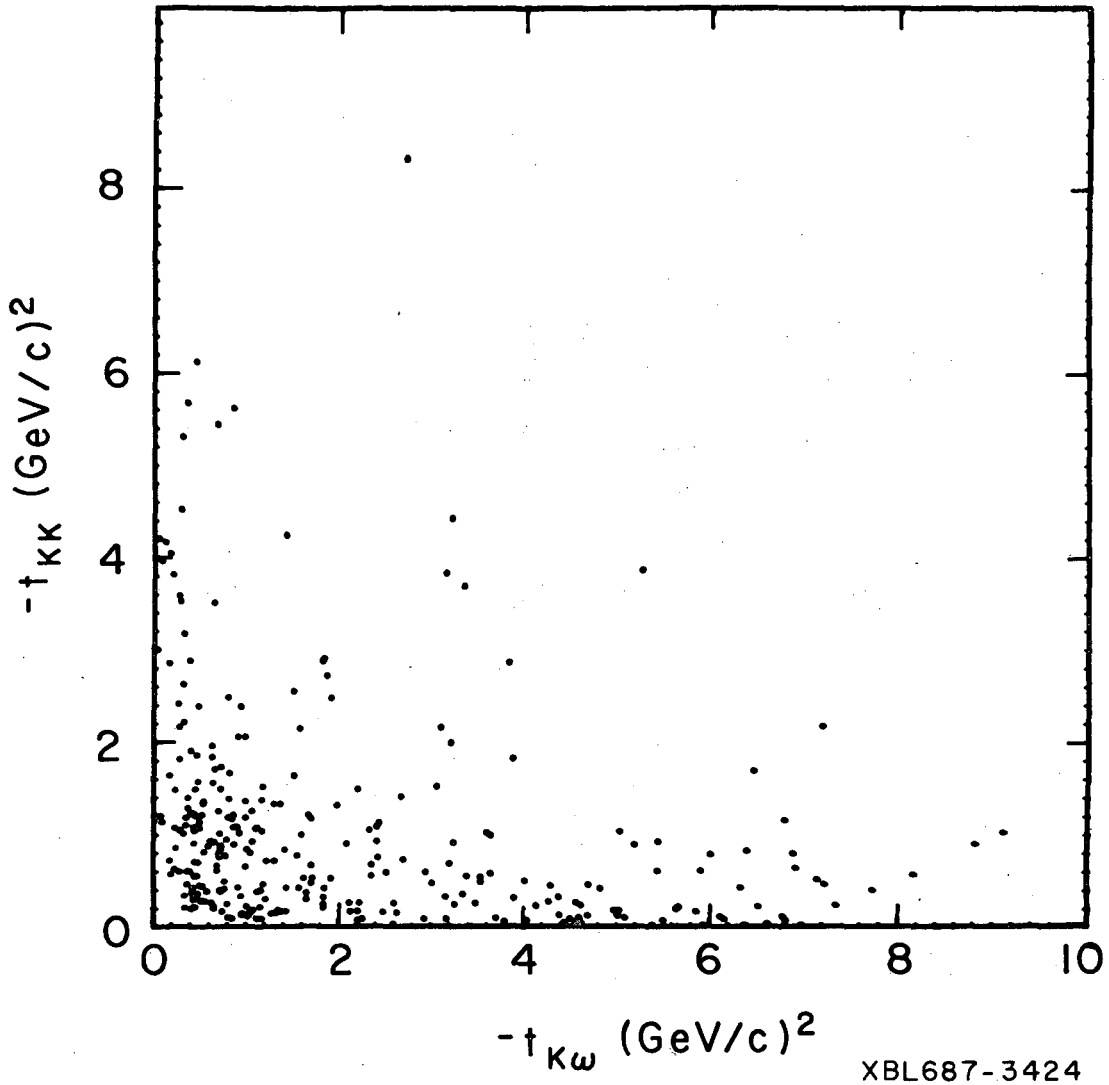
Fig. 14. Scatter plot of t_{KK} vs $t_{K\omega}$ for the 296 $K^+p \rightarrow K^+\omega p$ events at 9.0 GeV/c assigned to diagrams I and II of Fig. 13b.
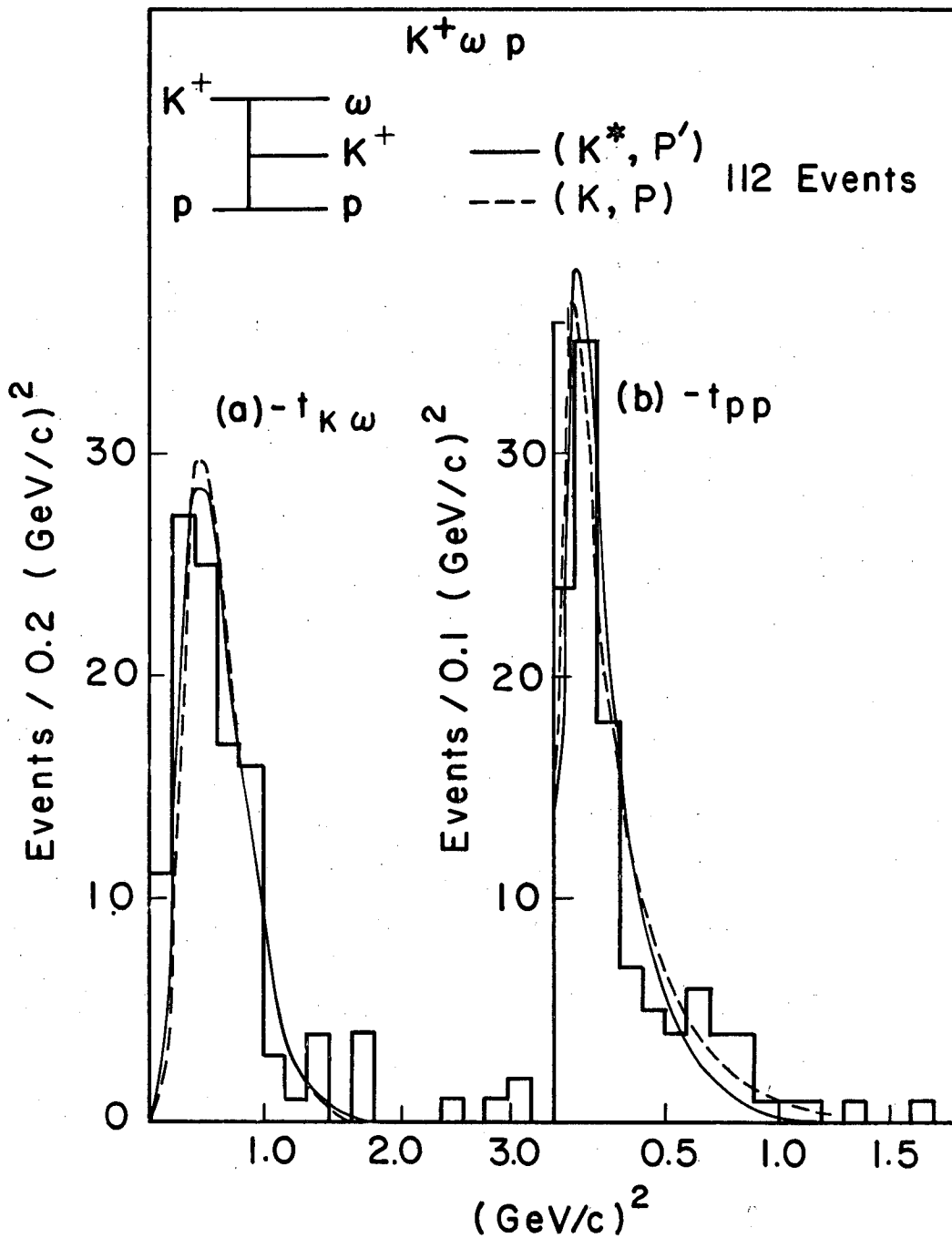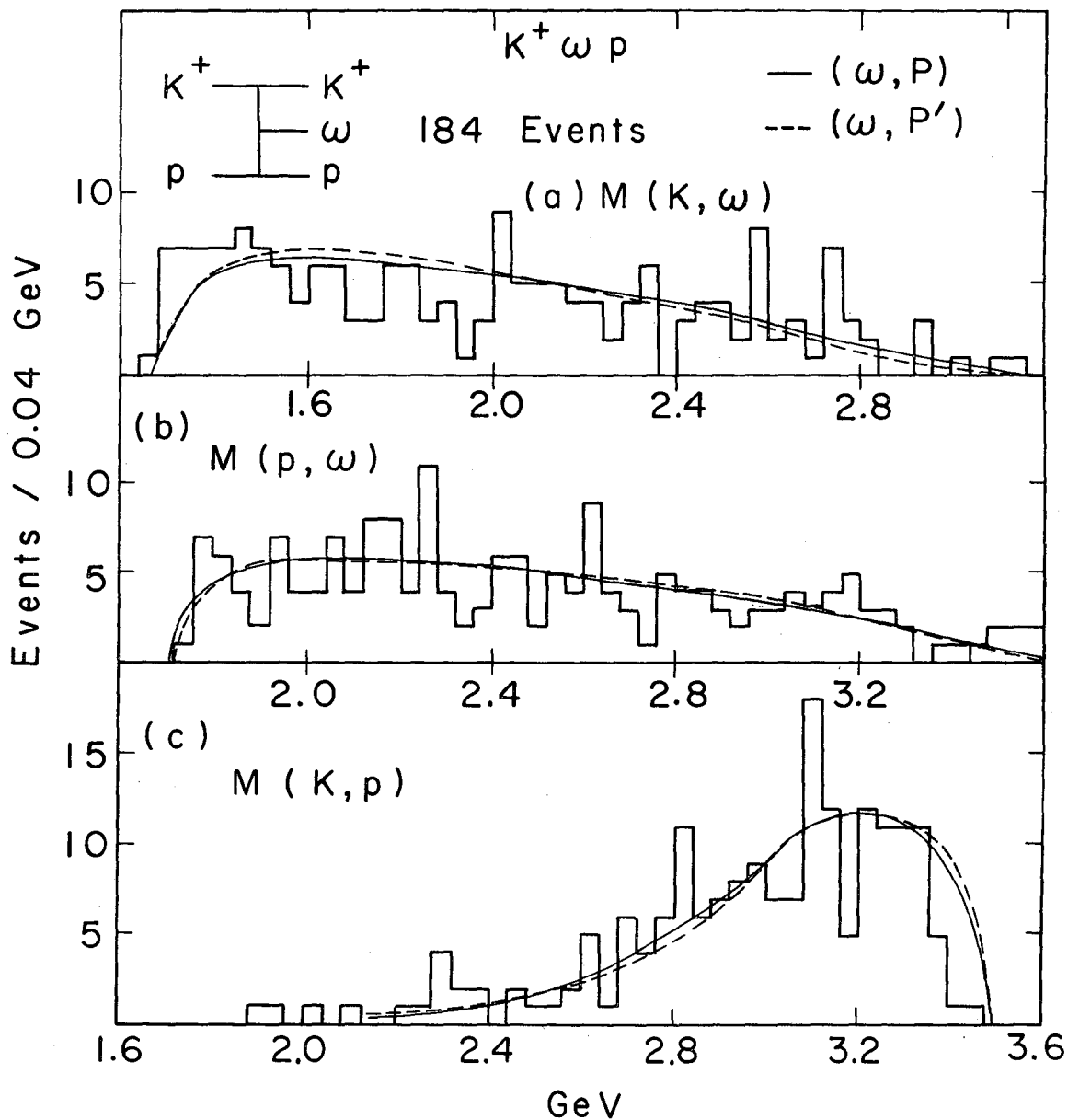
Fig. 15. Four momentum transfer distributions for the 112 $K^+p \rightarrow K^+\omega p$ events at 9.0 GeV/c assigned to diagram II of Fig. 13b. The solid and dashed lines represent the expected distribution from the double peripheral model with exchange trajectory pairs (K^*, P') and (K, P) respectively. (a) $t_{K\omega}$ and (b) t_{pp}.
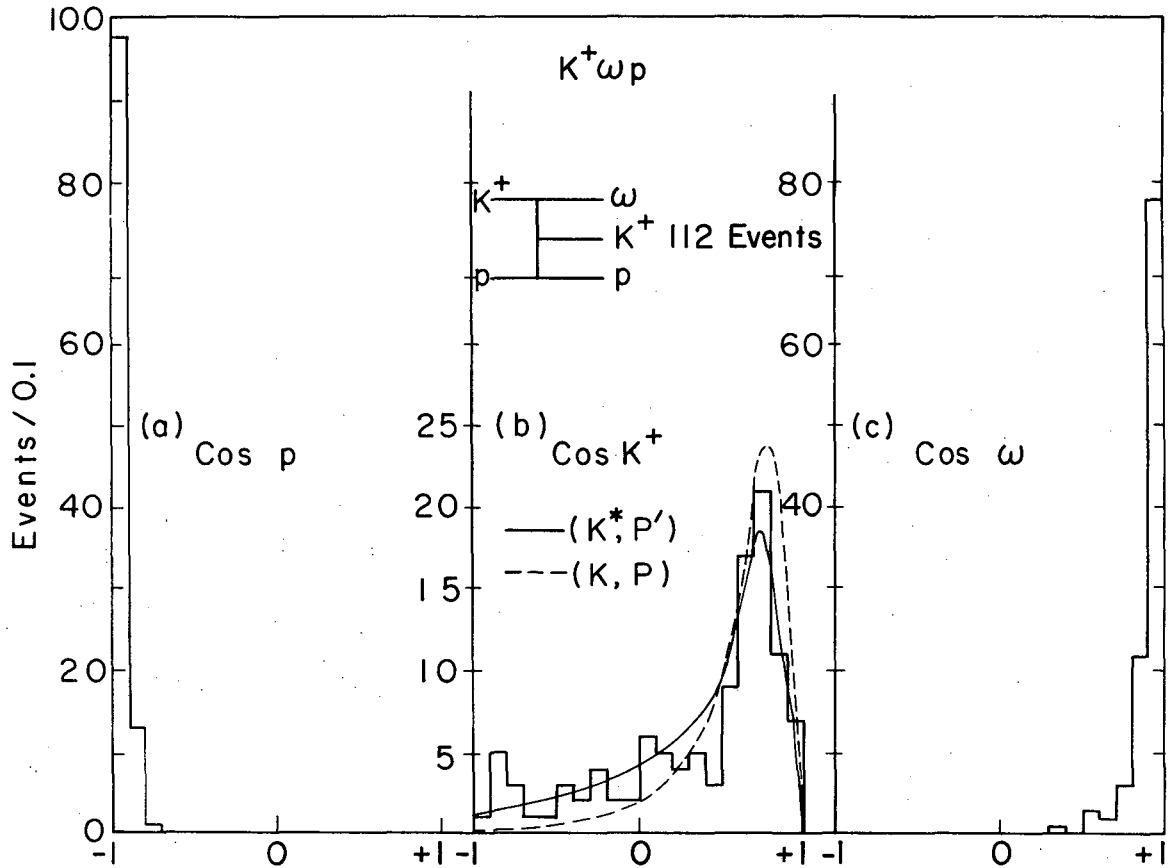
XBL687- 3379

Fig. 16. Angular distributions in the production center-of-mass system for the 112 $K^+p \to K^+\omega p$ events at 9.0 GeV/c assigned to diagram II of Fig. 13b. (a) $\cos \theta_p$; (b) $\cos \theta_{K^+}$, the solid and dashed lines are the expected distributions from the double peripheral model with the exchange trajectory pairs (K^*, P') and (K, P) respectively; (c) $\cos \theta_\omega$.
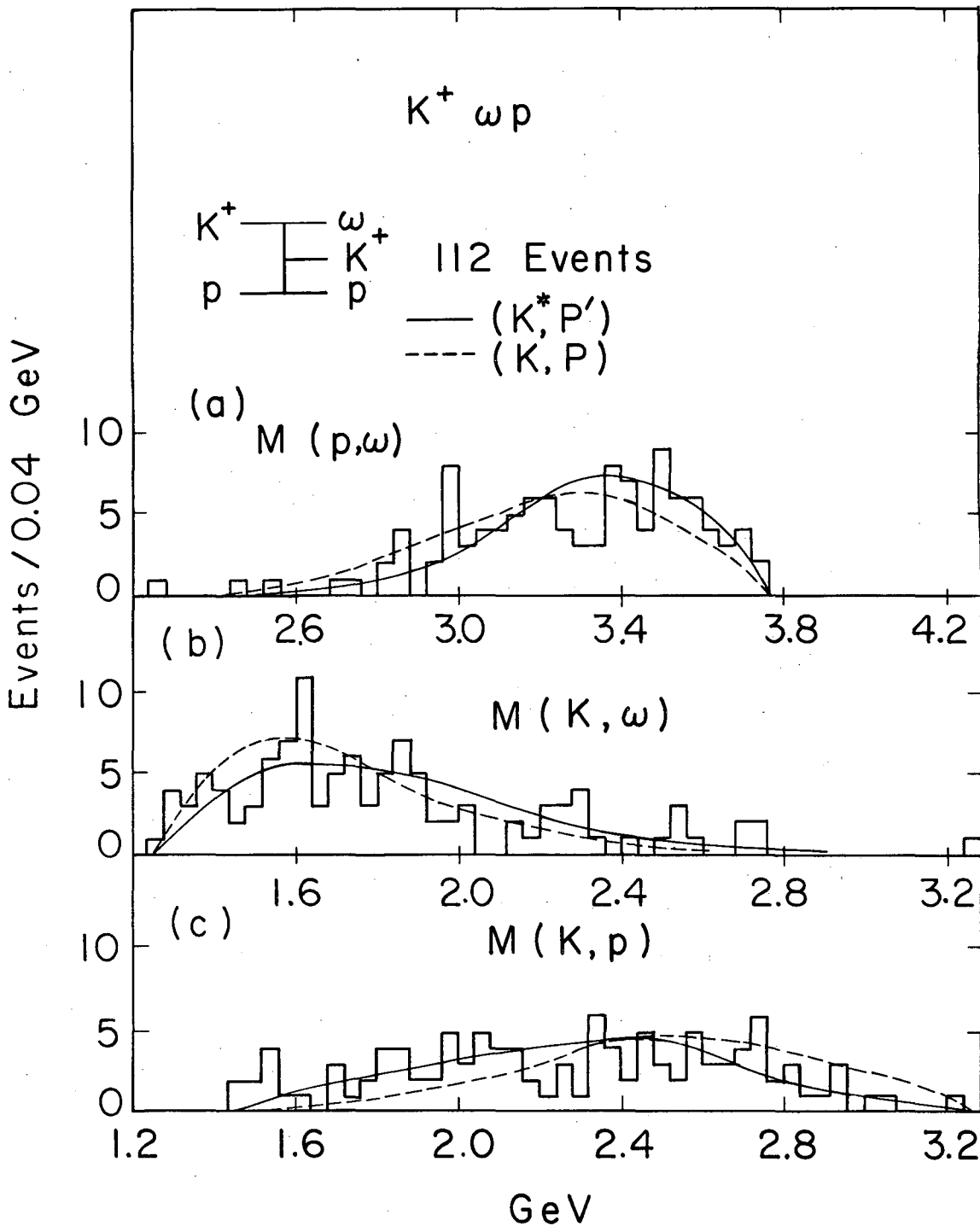
Fig. 17. Invariant mass distributions of the 112 $K^+p \rightarrow K^+\omega p$ events at 9.0 GeV/c assigned to diagram II of Fig. 13b. The solid and dashed curves represent the expected distributions from the double peripheral model with exchange trajectory pairs (K^*, P') and (K, P) respectively. (a) M(p, ω), (b) M(K^+, ω), and (c) M(K^+, p).
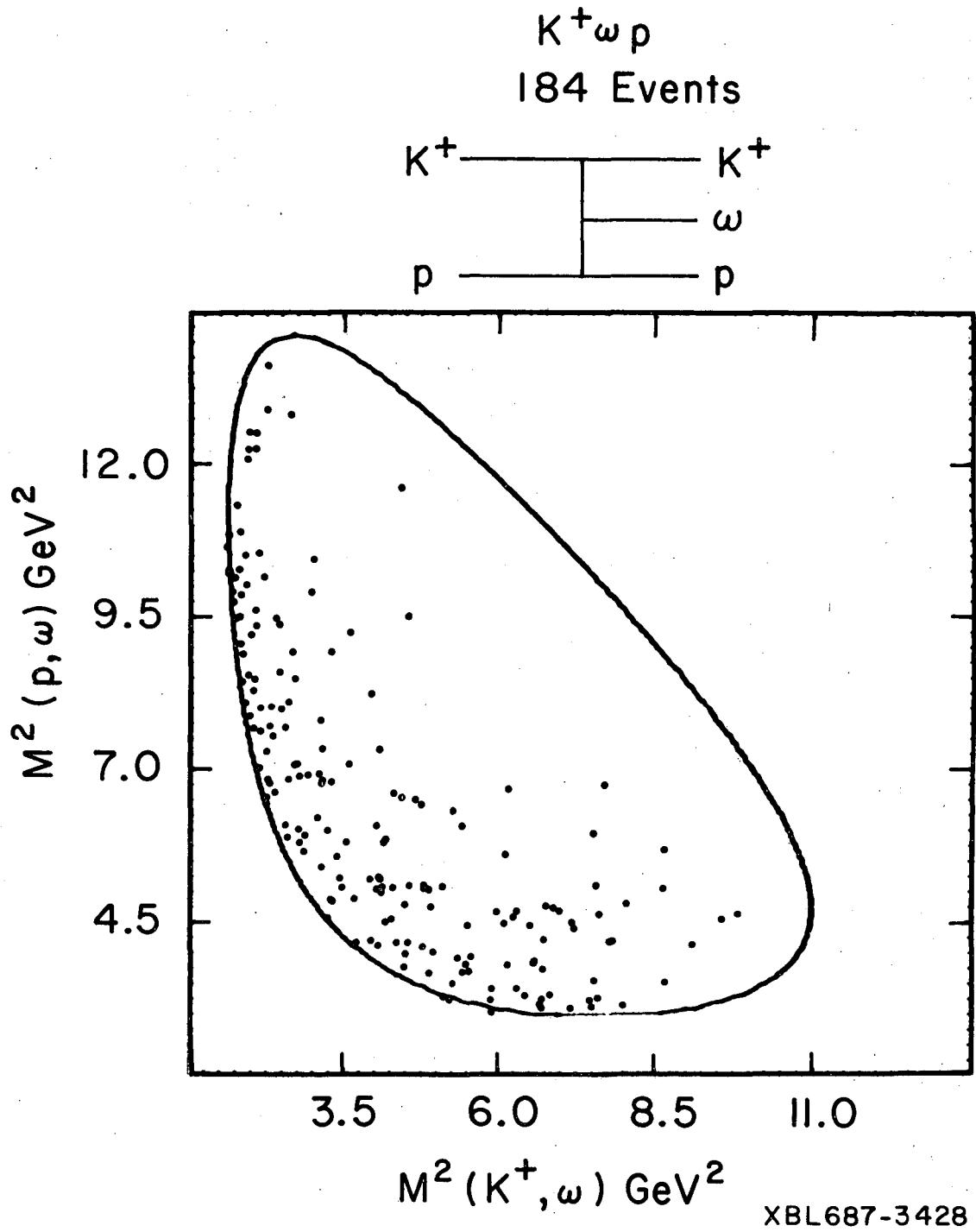
$K^+ \omega p$

112 Events
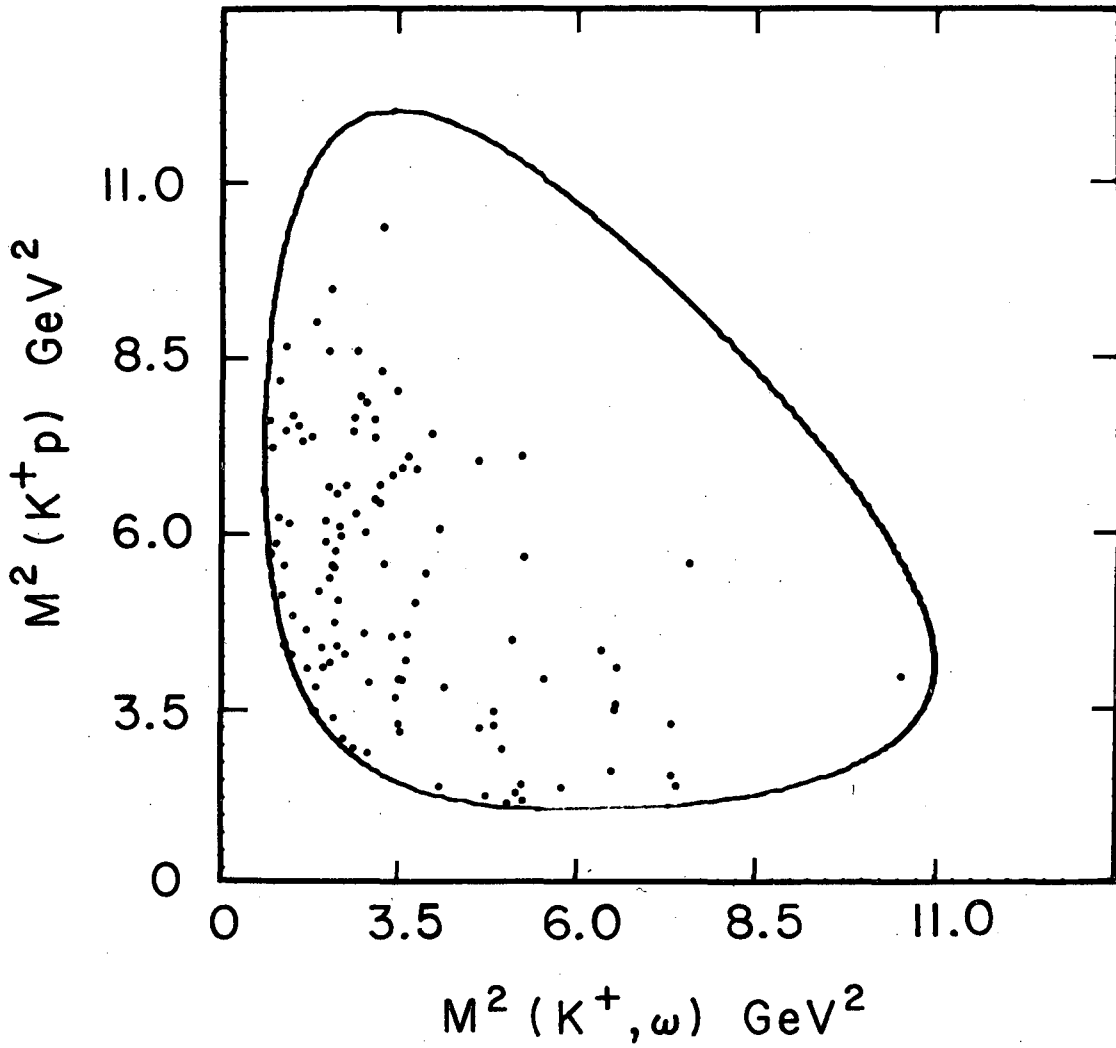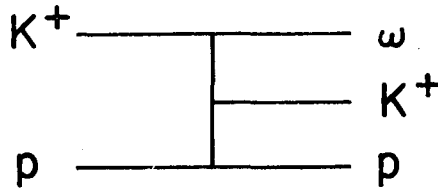
Fig. 18. The Dalitz plot of $M^2(K^+, p)$ vs $M^2(K^+, \omega)$ for the 112 $K^+ p \to K^+ \omega p$ events at 9.0 GeV/c assigned to diagram II of Fig. 13b.

XBL687-3427
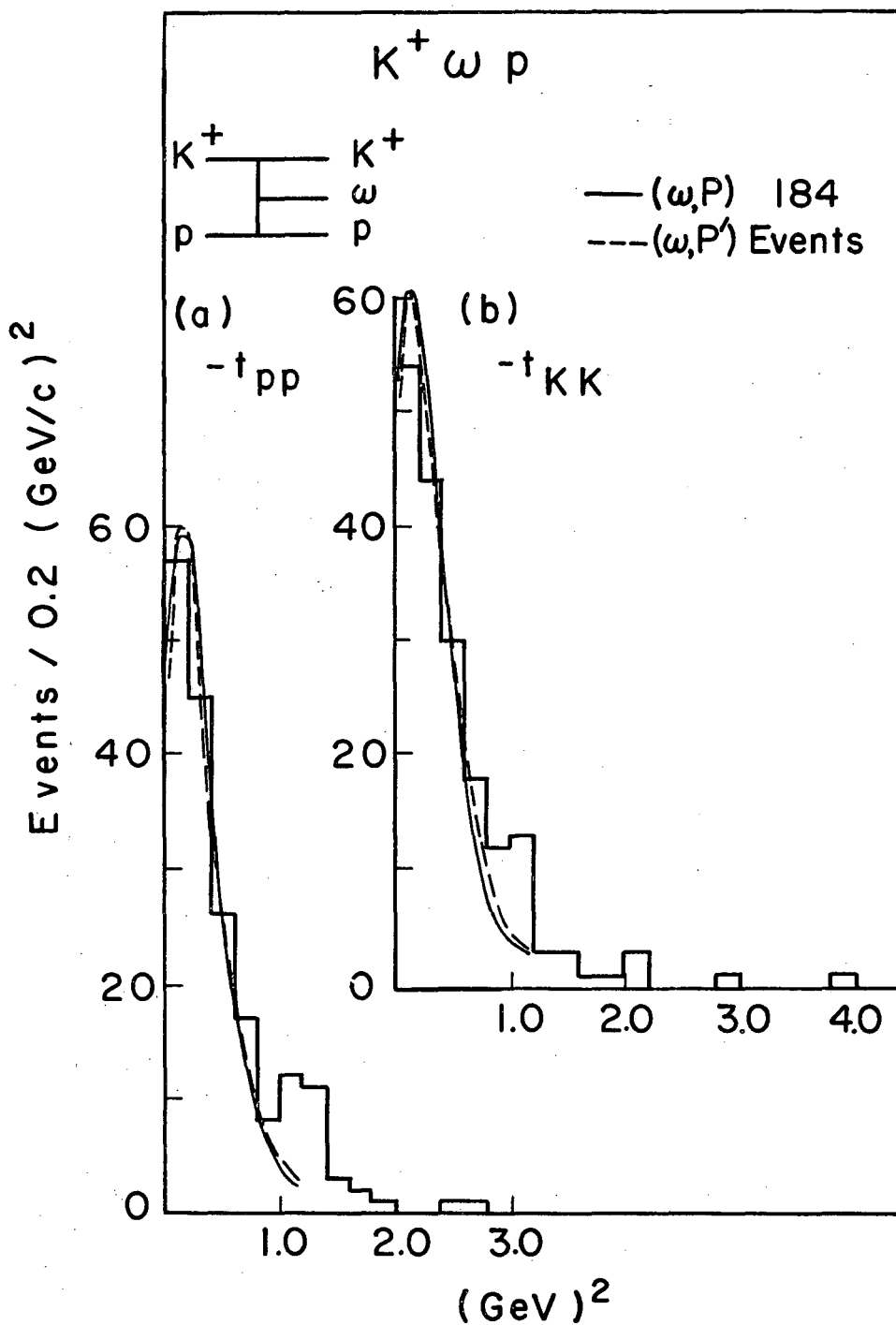
Fig. 19. Four momentum transfer distributions for the 184 $K^+ p \to K^+ \omega p$ events at 9.0 GeV/c assigned to diagram I of Fig. 13b. Solid and dashed lines represent the expected distributions from the double peripheral model with exchange trajectory pairs (ω, P) and (ω, P') respectively. (a) t_{pp} and (b) t_{KK}.
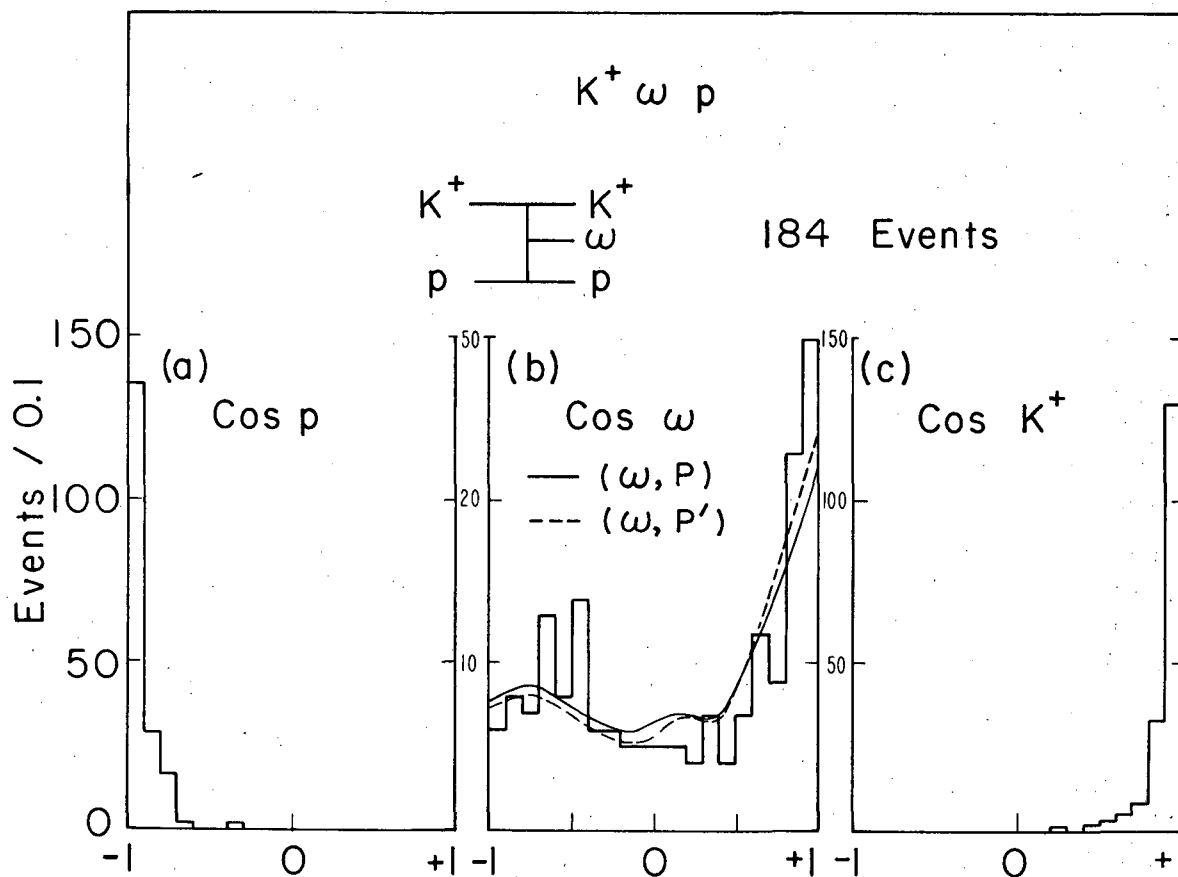
XBL687-3387

Fig. 20. · Angular distribution in the production center-of-mass system for the 184 $K^+ p \rightarrow K^+ \omega p$ events at 9.0 GeV/c assigned to diagram I in Fig. 13b. (a) $\cos \theta_p$; (b) $\cos \theta_\omega$, the solid and dashed lines are the expected distributions from the double peripheral model with the exchange trajectory pairs (ω, P) and (ω, P') respectively; (c) $\cos \theta_{K^+}$.

Fig. 21. Invariant mass distributions of the 184 $K^+p \rightarrow K^+\omega p$ events at 9.0 GeV/c assigned to diagram I in Fig. 13b. The solid and dashed lines represent the expected distributions from the double peripheral model with exchange trajectory pairs (ω, P) and (ω, P') respectively. (a) $M(K^+, \omega)$, (b) $M(p, \omega)$, and (c) $M(K^+, p)$.
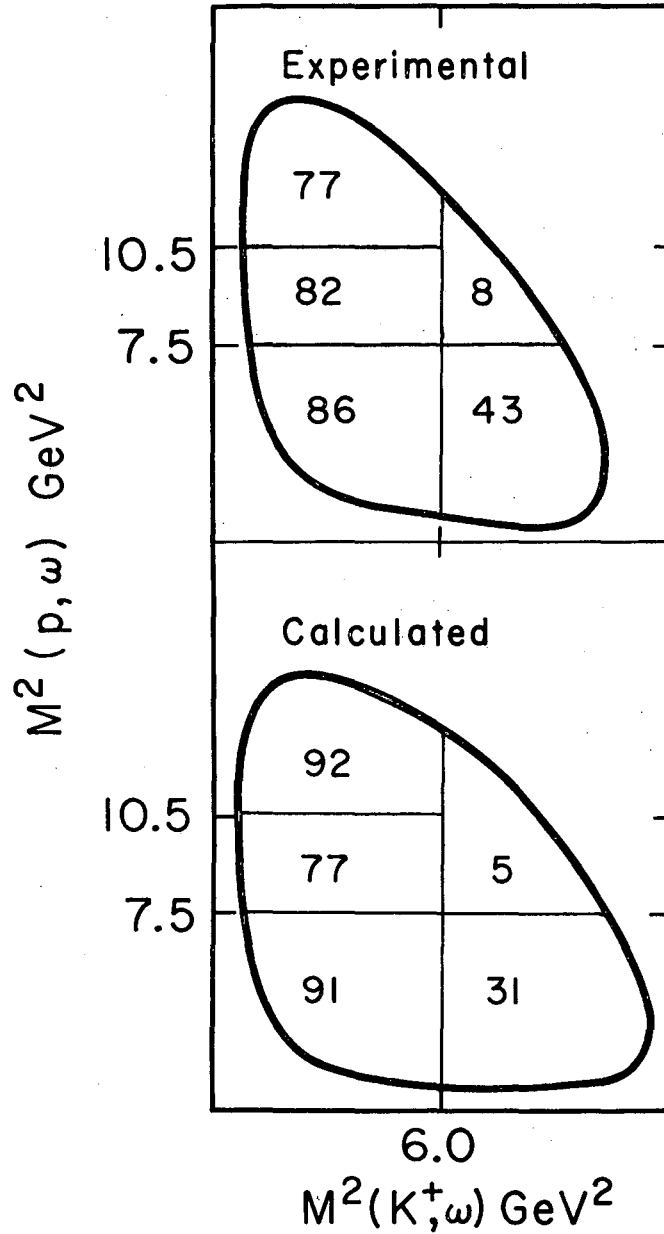
XBL687-3385

Fig. 22. The Dalitz plot of $M^2(p, \omega)$ vs $M^2(K^+, \omega)$ for the 184 $K^+p \to K^+\omega p$ events at 9.0 GeV/c assigned to diagram I of Fig. 13b.
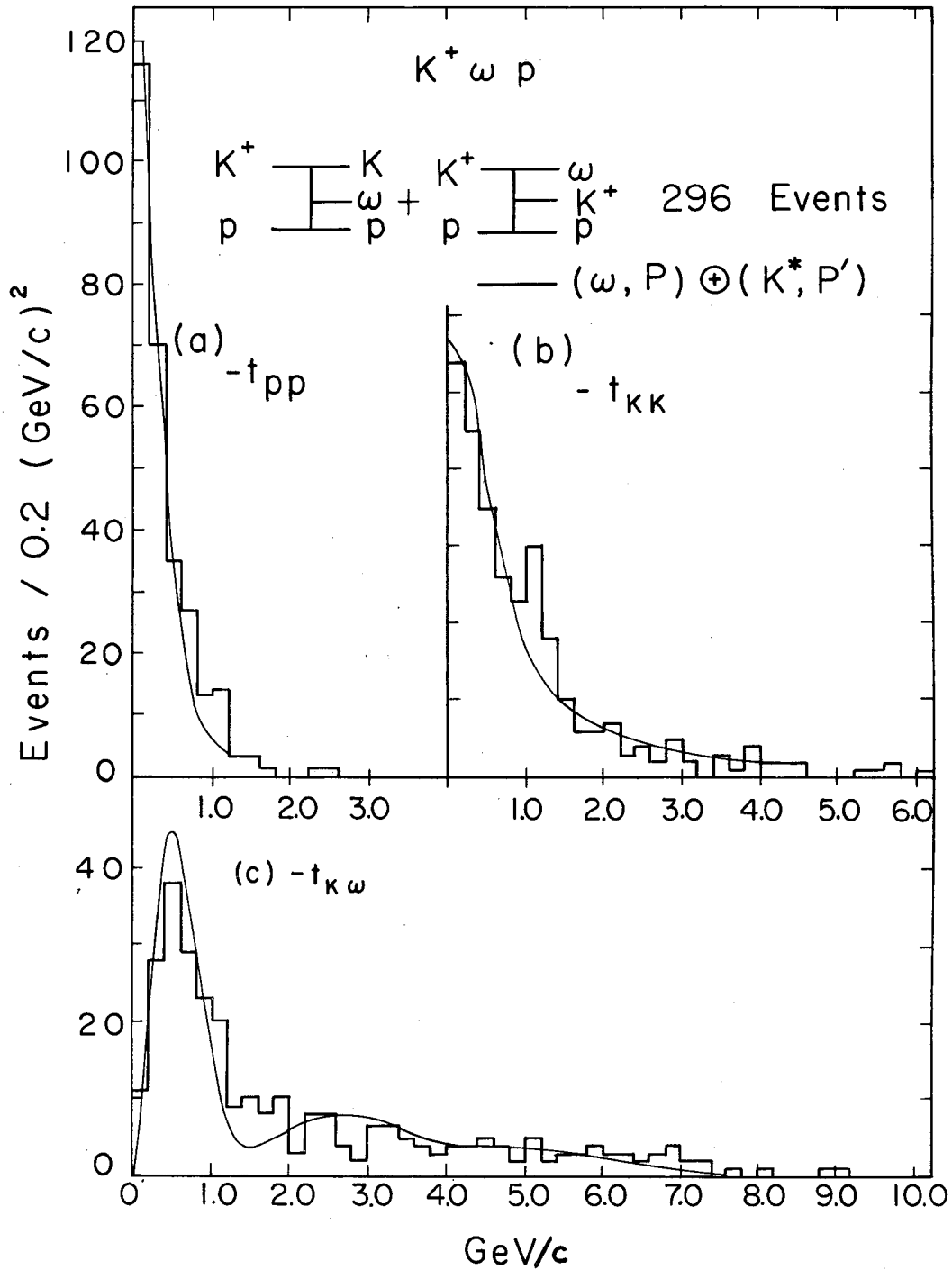
Fig. 23. Four momentum transfer plots for the 296 $K^+p \rightarrow K^+\omega p$ events assigned to either diagram I or diagram II of Fig. 13b. The solid curves are the expected distributions from the double peripheral model adding together diagrams I and II using the exchange trajectory pairs (ω, P) for diagram I and (K^*, P') for diagram II. (a) t_{pp}, (b) t_{KK}, and (c) $t_{K\omega}$.
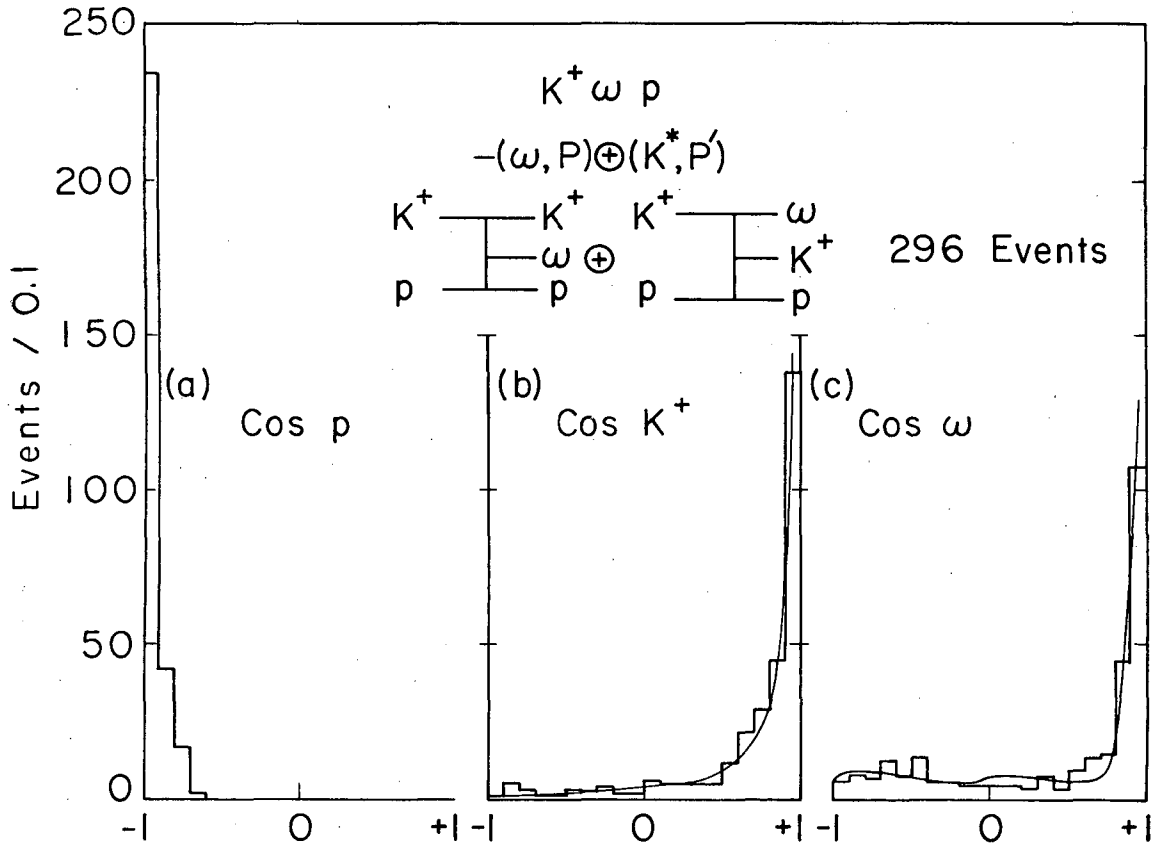
XBL687-3382

Fig. 24. Angular distributions in the production center-of-mass system for
the 296 $K^+ p \rightarrow K^+ \omega p$ events at 9 GeV/c assigned to either diagram I or
diagram II shown in Fig. 13b. The solid curves represent the expected
distribution from the double peripheral model adding together diagrams I
and II using the exchange trajectory pairs (ω, P) for diagram I and (K^*, P')
for diagram II. (a) $\cos \theta_p$, (b) $\cos \theta_{K^+}$, and (c) $\cos \theta_\omega$.
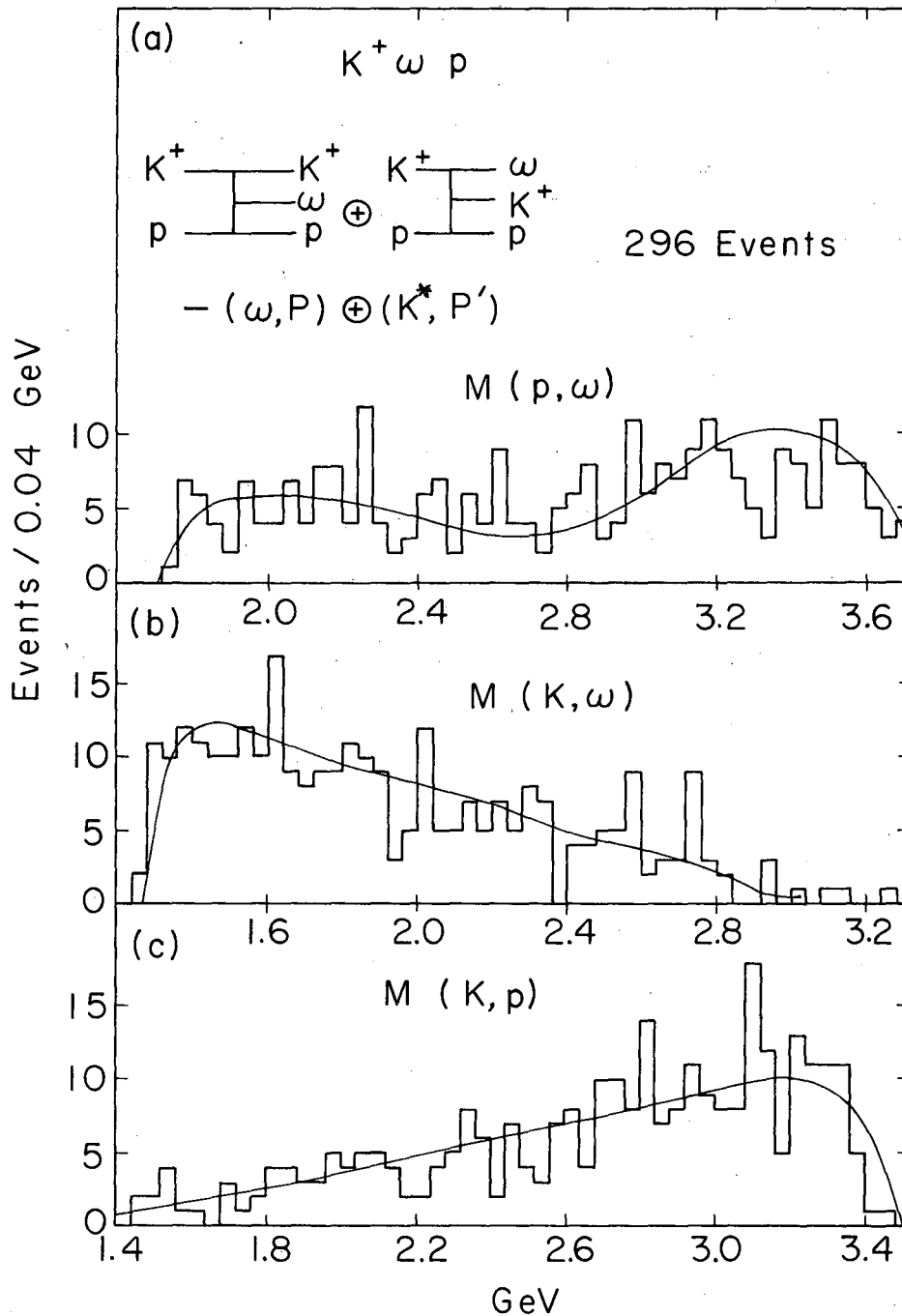
XBL 687-3384

Fig. 25. Invariant mass distributions of the 296 $K^+ p \rightarrow K^+ \omega p$ events assigned

either to diagram I or II of Fig. 13b. The solid lines represent the

expected distributions from the double peripheral model adding together

diagrams I and II and using the exchange trajectory pairs (ω, P) for

diagram I and (K^*, P') for diagram II. (a) $M(p, \omega)$, (b) $M(K^+, \omega)$, and
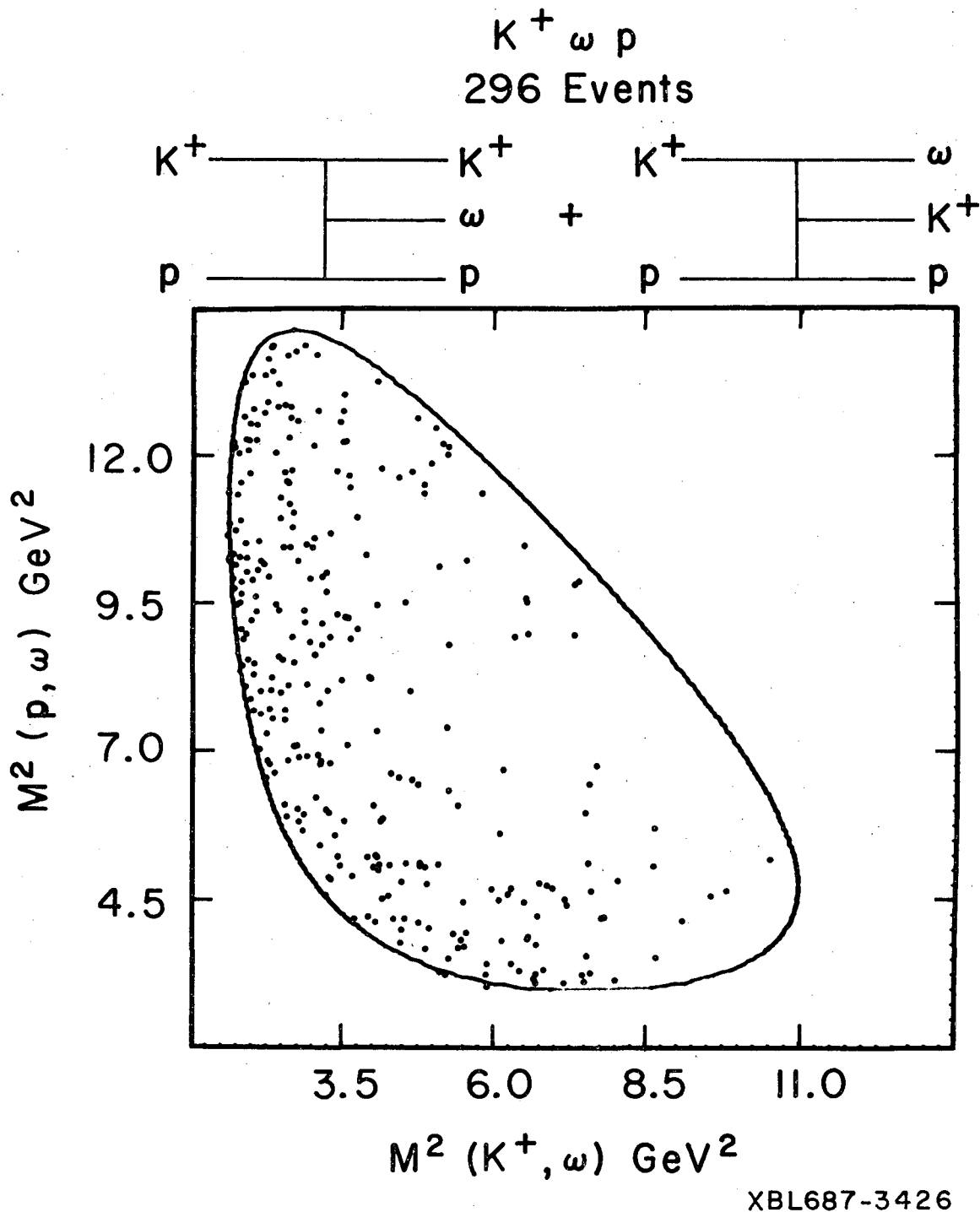
Fig. 26. (a) $M^2(p, \omega)$ vs $M^2(K^+, \omega)$ for the 296 $K^+p \to K^+\omega p$ events at 9.0

GeV/c assigned to either diagram I or II of Fig. 13b. (b) Comparison

between the experimental Dalitz plot distribution and the one calculated

from the double peripheral Regge model using the parameters given in Table II.

Fig. 26b.